Immunocytochemistry

The cells were fixed with 4% paraformaldehyde for 10 minutes and then blocked with 3% goat serum in phosphate-buffered saline containing 0.1% Triton X-100 for 30 minutes. The cells were incubated for 2 hours with one or two of the following specific primary antibodies at the stated dilutions: mouse monoclonal anti–Ki-67 (1:200; BD Biosciences, Franklin Lakes, NJ, http://www.bdbiosciences.com) as a cell-division marker; rat monoclonal anti-BrdU (1:40; Abcam, Cambridge, UK, http://www.abcam.com) as an S-phase cell marker; rabbit antiactive caspase-3 (1:200; BD Biosciences) as a cell-death marker; mouse monoclonal antirhodopsin (1:200; Chemicon International, Temecula, CA, http://www.chemicon.com/) as a rod photoreceptor cell marker; mouse monoclonal antisyntaxin (1:200; Sigma-Aldrich) and rabbit polyclonal anti-Pax6 (1:500; Chemicon International) as amacrine cell markers; mouse monoclonal antiglutamine (Gln) synthetase (1:200; Chemicon International) as a Müller glia marker; and mouse monoclonal anti–β-catenin (1:250; BD Biosciences). The cells were examined by epifluorescence after incubation for 30 minutes in Alexa 488- and/or Alexa 596-conjugated secondary antibodies (Molecular Probes, Eugene, OR; http://www.probes.com). Cell nuclei were counterstained with Hoechst 33258 (Nacalai Tesque, Kyoto, Japan, http://www.nacalai.co.jp). Negative controls were performed in parallel during all immunocytologic processing by omission of a primary antibody. No fluorescent labeling was observed in the negative controls. Images were obtained using an AX70 fluorescence microscope (Olympus, Tokyo, http://www.olympus-global.com) or TCS SP2 AOBS confocal microscope (Leica Microsystems, Wetzlar, Germany, http://www.leica-microsystems.com).

Statistical Analysis

The data represent the mean ± standard deviation of three separate experiments. For cytochemical studies, five randomly selected fields per sample were analyzed in each condition. Statistical significance was determined by Student's two-tailed *t*-test.

Results

Stem Cell Properties of Ciliary Margin Cells

To ensure the existence of retinal stem cells from the ciliary margins of 8-week-old mice, the dissociated ciliary margin cells were cultured in the nonadherent condition at a clonal density. After 5 days in culture, sphere formation was observed. To further examine whether these sphere colonies were generated by the proliferation of single cells, ciliary margin cells were prepared from both GFP-expressing and wild-type mice, and the cell mixture was cultured at a clonal density for 5 days according to the method of Tropepe et al. [9]. Separate GFP-positive and GFP-negative spheres were observed (Fig. 1), demonstrating that the colonies were not derived from cell aggregation but instead arose clonally. Green spheres contained some dark dots, which might look like GFP-negative cells. However, they were not actually GFP-negative cells but differentiated pigment epithelial cells whose pigment may mask or impede the green color. These sphere cells were capable of generating secondary spheres and differentiating to express different retinal cell–specific markers, rhodopsin, syntaxin, and Pax6, under culture conditions that promoted retinal cell differentiation [8] (Table 1). Thus, the sphere cells from the ciliary margin possessed the stem cell characters of self-renewal and multilineage potential.

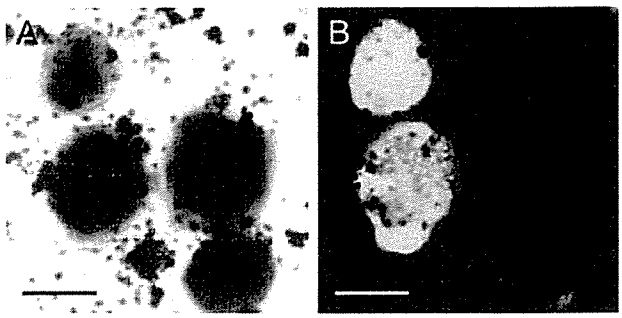

Figure 1. Clonal sphere formation of retinal stem cells from the adult ciliary margin. Phase **(A)** and fluorescence **(B)** photomicrographs are shown. Dissociated adult ciliary margin cells from GFP-expressing and wild-type mice were mixed and cultured in the nonadherent condition for 5 days. The mixture of dissociated cells generated distinctive spheres. Scale bars = 100 μm.

Effect of Wnt3a on Cell Proliferation

Because a limited number of primary spheres can be generated from individual adult eyes, improved and efficient strategies that expand the retinal stem cell pool by promoting cell proliferation are required. Wnt is a good candidate for this because it acts as a mitogen for immature retinal cells [18]. We first examined the

Table 1. Sphere cells expanded by Wnt3a or SB216763 retained their multilineage potential

	FGF2	Wnt3a	SB216763
Rhodopsin	10.2 ± 1.8	12.3 ± 2.4	10.6 ± 3.9
Syntaxin/Pax6	4.7 ± 1.2	3.9 ± 1.3	5.1 ± 0.2
Gln Synthetase	24.0 ± 5.6	24.0 ± 10.0	26.3 ± 10.4

The average percentage (± standard deviation) of cell types in the number of nuclei stained with Hoechst is shown in the column. Sphere colonies were grown in fibroblast growth factor 2 (FGF2)-, Wnt3a-, orSB216763-containing medium for 5 days. Thereafter, each sphere colony was plated and cultured for 21 days under conditions that promote retinal cell differentiation. The sphere-derived cells expressed several retinal cell–specific markers, such as rhodopsin as rod photoreceptors, Pax6 and syntaxin as amacrine cells, or Gln synthetase as Müller glia. In respect of these markers, any marked deviation of retinal cell fate was not observed among conditions of sphere formation.

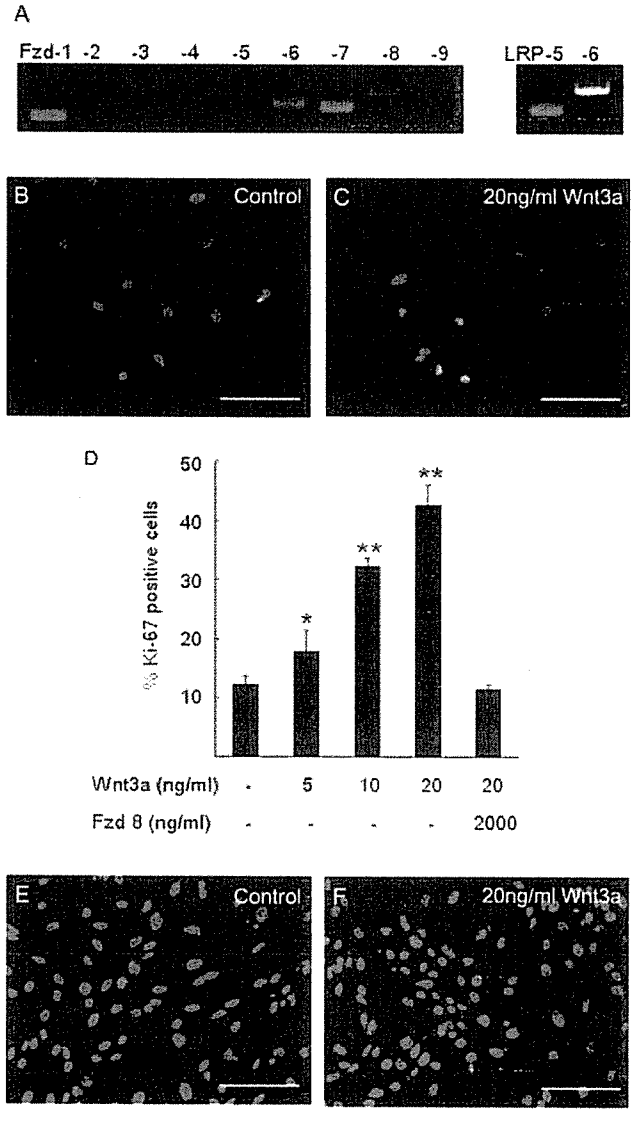

Figure 2. Effect of Wnt3a on the cell-division markers. **(A):** Expression of Fzd family and LRP-5/6 mRNAs in the primary sphere cells were examined by reverse transcription–polymerase chain reaction. Gene products specific for Fzd-1, -3, -4, -6, -7, and -8 and LRP-5 and -6 were amplified. **(B–F):** Primary spheres were triturated and cultured in the adherent condition with various concentrations of Wnt3a for 48 hours. In the control cultures, 2.5 μg/ml dimethyl sulfoxide was added to the medium. The fluorescence photomicrographs **(B, C)** show merged images of Hoechst (blue) and anti–Ki-67 antibody (green) labeling. The number of Ki-67–positive cells in the culture containing 20 ng/ml Wnt3a **(C)** is greater than that in the control culture **(B)**. Quantification of Ki-67–positive cells **(D)** shows that Ki-67–positive cells increase in a Wnt3a dose-dependent manner, and Fzd-8-CRD (a Wnt antagonist) blocks this effect. All data represent the means ± standard deviations of three separate experiments. The fluorescence photomicrographs **(E, F)** show merged images of Hoechst (blue) and anti-bromodeoxyuridine (BrdU) antibody (red). In the presence of Wnt3a, the number of BrdU-incorporating cells is greater than that in the control condition. Scale bars = 100 μm. $^*p < .05$, $^{**}p < .01$ compared with control cultures.

expression of Wnt receptor genes in the sphere cells by reverse transcription–PCR. As shown in Figure 2A, gene products specific for Fzd-1, -3, -4, -6, -7, and -8 were amplified, whereas no signals for Fzd-2, -5, and -9 were detected. LRP-5 and -6, which are known to be indispensable receptors for the canonical Wnt pathway, were expressed. These results suggest that sphere cells from the adult ciliary margin have the prerequisites to react in response to Wnt proteins. To address the effect of Wnt signaling on the proliferation of adult retinal stem cells, the spheres were dissociated and cultured in the adherent condition for 48 hours in the presence of recombinant Wnt3a at a series of graded concentrations. The proliferative response was assayed by immunocytochemical staining for Ki-67, a cell-division marker [23]. Ki-67-positive cells were increased in a dose-dependent manner after the addition of Wnt3a (Figs. 2B–2D). This effect was maximal at 20 ng/ml Wnt3a, when the Ki-67-positive cells increased by 3.5-fold compared with control cultures. Since the recombinant Wnt3a used was only refined to 75% purity according to the manufacturer's description, there was a possibility that some of the impurities could have influenced the cell proliferation. Thus, Fzd-8-CRD, a Wnt antagonist [24, 25], was applied to the dissociation culture together with the recombinant Wnt3a. Sufficient dose of Fzd-8-CRD decreased the number of Ki-67–positive cells to the basal level (Fig. 2D), confirming the mitogenic effect of Wnt3a on sphere-derived cells. To examine DNA synthesis in the sphere-derived cells, they were pulse-labeled with BrdU for 4 hours. In the presence of 20 ng/ml Wnt3a, the number of BrdU-positive cells was increased from 10.2% ± 2.5% to 18.8% ± 1.6% ($p < .01$) (Figs. 2E, 2F), consistent with the increase in Ki-67–positive cells. Under all of the above conditions, there was no difference in the cell death estimated by immunocytochemical detection of activated caspase-3 (data not shown).

To further estimate the proliferative response, we assessed the size of the primary spheres (50 μm or more of the diameter) with or without Wnt3a. After a 5-day culture in vitro, the diameter of the spheres was increased in the presence of 20 ng/ml Wnt3a (Fig. 3A), consistent with the data in the adherent condition described above. Notably, the average volume of the Wnt3a-treated spheres was threefold larger than that of the control spheres, although various sizes of spheres appeared in Wnt3a-containing cultures. To exclude the possibility that Wnt3a increased each cell volume, the nuclei of sphere cells were stained by Hoechst 33258 and the cell densities were examined by the confocal microscope. The cell densities of the Wnt3a-treated spheres were nearly equal to those of control spheres (Figs. 3B, 3C), confirming that the size of the spheres was reflected in the cell number but not the cell size. On the

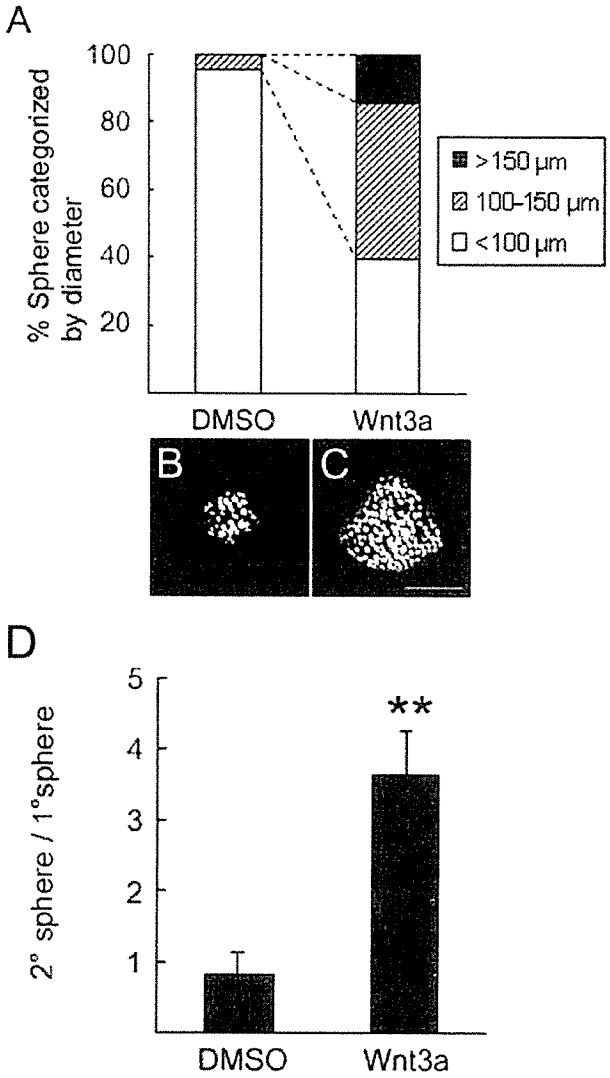

Figure 3. Effect of Wnt3a on the sphere formation. **(A):** Percentages of spheres categorized by their diameter. Isolated ciliary margin cells were plated at 20,000 cells/ml and cultured in the nonadherent condition with 20 ng/ml Wnt3a for 5 days, and the sphere size was estimated. In the control cultures, 2.5 μg/ml dimethyl sulfoxide (DMSO) was added to the medium. A large proportion of spheres in the Wnt3a-containing culture are greater than 100 μm in diameter, whereas most of the spheres in the DMSO-treated control culture have diameters of 100 μm or less. The results are representative of three independent experiments. The percentages of sphere-forming cells with DMSO and Wnt3a were 0.098% ± 0.02% and 0.12% ± 0.03%, respectively. **(B, C):** Confocal microscopic images of the nuclei-counterstained primary spheres. The cell densities of the Wnt3a-induced large-sized spheres **(C)** were nearly equal to that of small-sized spheres in the control condition **(B)**. **(D):** Numbers of secondary spheres generated from primary spheres. Primary spheres were triturated and cultured in the nonadherent condition for 7 days in the presence of fibroblast growth factor 2 and epidermal growth factor. The number of secondary spheres generated from Wnt3a-treated spheres is greater than that from DMSO-treated control spheres. The results are the means ± standard deviations of three replicates. Scale bar = 100 μm. $^{**}p < .01$ compared with control cultures.

contrary, there was no significant difference between the number of primary sphere colonies in the Wnt3a-containing and control cultures (data not shown), suggesting that Wnt3a did not affect the number of cells capable of forming primary spheres nor transform nonsphere forming cells into sphere-forming stem cells. Taken together, Wnt3a promotes the proliferation of sphere-forming cells from the adult ciliary margin.

Characterization of Cells Expanded by Wnt3a

Although Wnt3a promoted the proliferation of sphere cells, it remained unclear whether this proliferation was accompanied by self-renewal of the adult retinal stem cells. If Wnt3a promoted self-renewal, the Wnt3a-treated cells should retain their stem cell characters even after proliferation. To test this hypothesis, individual primary sphere colonies cultured in the presence or absence of Wnt3a were dissociated and allowed to form secondary spheres. The Wnt3a-treated cells generated fourfold the number of secondary sphere colonies compared with dimethylsulfoxide (DMSO)-treated cells from a single primary sphere (Fig. 3D). In parallel with the increased sphere size after Wnt3a treatment, the Wnt3a-treated spheres contained greater numbers of stem cells than the control DMSO-treated spheres, indicating that Wnt 3a promotes proliferation of sphere-derived cells, including retinal stem cells.

To further characterize the cells expanded by Wnt3a, we next examined the multilineage potential of Wnt3a-treated cells. Sphere colonies grown in Wnt3a-containing medium were dissociated and cultured for 7 days under conditions that promote retinal cell differentiation as described above. The Wnt3a-treated cells expressed several retinal cell–specific markers, such as rhodopsin as rod photoreceptors (Fig. 4A), Pax6 and syntaxin as amacrine cells (Fig. 4B), or Gln synthetase as Müller glia (Fig. 4C). In respect of these markers, Wnt3a-treated cells did not show any marked deviation of retinal cell fate compared with FGF2-treated cells (Table 1). Thus, sphere cells expanded by Wnt3a retained their multilineage potential.

Activation of the Canonical Wnt Pathway

To investigate whether Wnt3a protein activates the canonical Wnt pathway in sphere-derived cells from the adult ciliary margin, we next examined the subcellular localization of β-catenin by immunocytochemistry. β-catenin is a coactivator of LEF/TCF-dependent transcription but is normally phosphorylated by GSK3β and quickly degraded. Activation of the canonical Wnt pathway inhibits the kinase activity of GSK3β, resulting in relocation of stabilized β-catenin to the nucleus. After trituration of primary spheres derived from the adult ciliary margin, the cells were cultured in the adhesive condition for 1 day and then treated with or without 20 ng/ml Wnt3a for 2 hours. The Wnt3a-treated cells showed nuclear accumulation of β-catenin (Fig. 5B, Wnt3a). In contrast, a low level of β-catenin was observed under

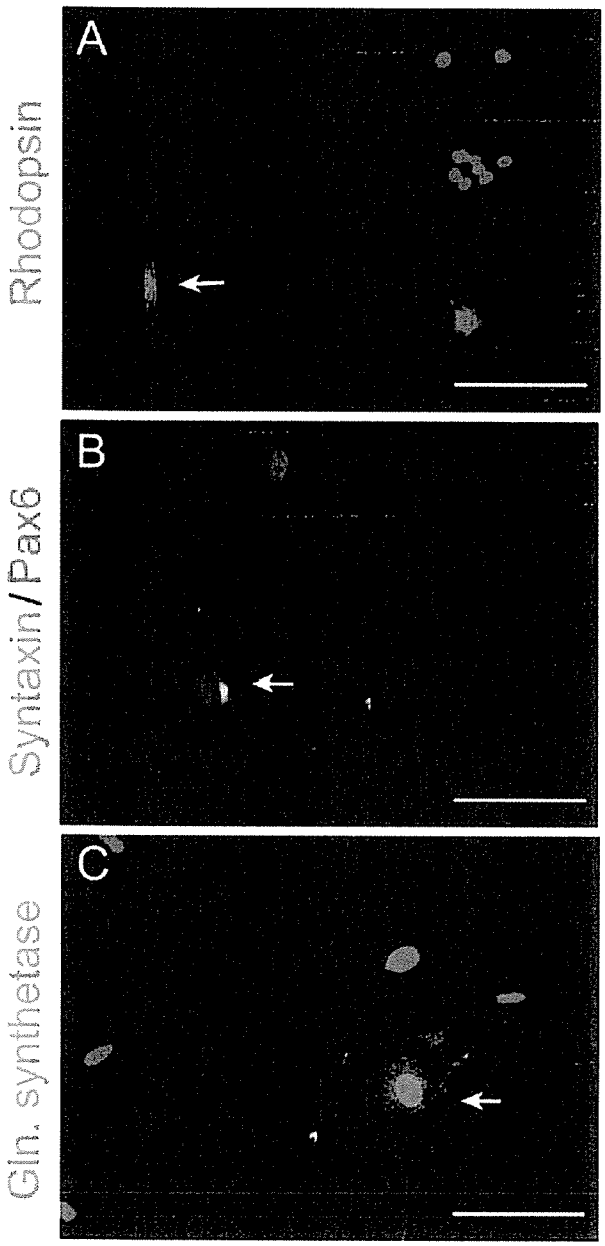

Figure 4. Fluorescence photomicrographs of differentiated cells. Wnt3a-treated sphere cells were triturated and cultured under conditions that promote retinal cell differentiation for 7 days. The Wnt3a-treated cells expressed several retinal cell–specific markers, such as rhodopsin as rod photoreceptors **(A)**, Pax6 and syntaxin as amacrine cells **(B)**, or glutamine (gln) synthetase as Müller glia **(C)**. Scale bars = 100 μm.

the plasma membrane and in the cytoplasmic region of nontreated cells (Fig. 5A, control). Thus, Wnt3a is capable of activating the canonical Wnt pathway in sphere-derived cells.

Effect of a GSK3 Inhibitor on Proliferation

Despite the activation of the canonical pathway by Wnt3a, it remained unclear whether its activation was involved in promoting the proliferation of sphere-derived cells. Thus, we investigated the effect of SB216763, a specific GSK3 inhibitor [26]. GSK3β is a key enzyme in the canonical Wnt pathway that destabilizes β-catenin, and thus SB216763 addition is supposed to mimic Wnt3a stimulation [17, 27]. SB216763 treatment of sphere-derived cell cultures increased Ki-67–positive cells in a dose-dependent manner (Fig. 6A). This effect was maximal at 2.5 μM, when the number of Ki-67–positive cells increased by twofold compared with control cultures. Moreover, the sphere size was increased by SB216763 addition (Fig. 6B). Thus, the GSK3 inhibitor alone mimicked the Wnt3a activity on the proliferation of sphere-derived cells, suggesting that activation of the canonical Wnt pathway was involved in the enhancement of proliferation of sphere-derived cells. Moreover, the SB216763-treated cells expressed several retinal cell–specific markers under conditions that promote retinal cell differentiation and did not show any marked deviation of retinal cell fate compared with FGF2-treated cells (Table 1). Thus, sphere cells expanded by SB216763 retained their multilineage potential.

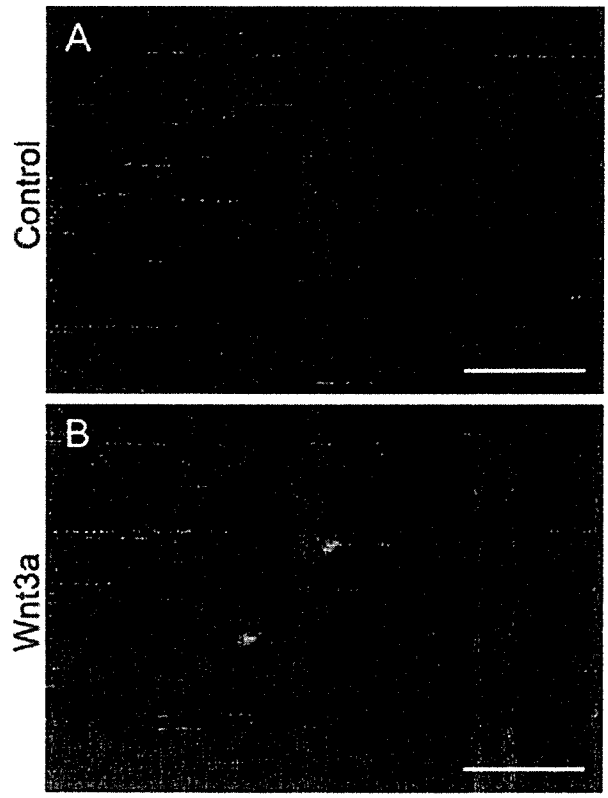

Figure 5. Nuclear translocation of β-catenin in the sphere-derived cells induced by Wnt3a. The localization of β-catenin was examined by immunohistochemistry at 2 hours after the addition of 2.5 μg/ml DMSO **(A)** or 20 ng/ml Wnt3a **(B)**. **(A):** β-catenin is observed in the cytoplasm and plasma membrane. **(B):** Wnt3a-treated cells show nuclear accumulation of β-catenin. Scale bars = 100 μm.

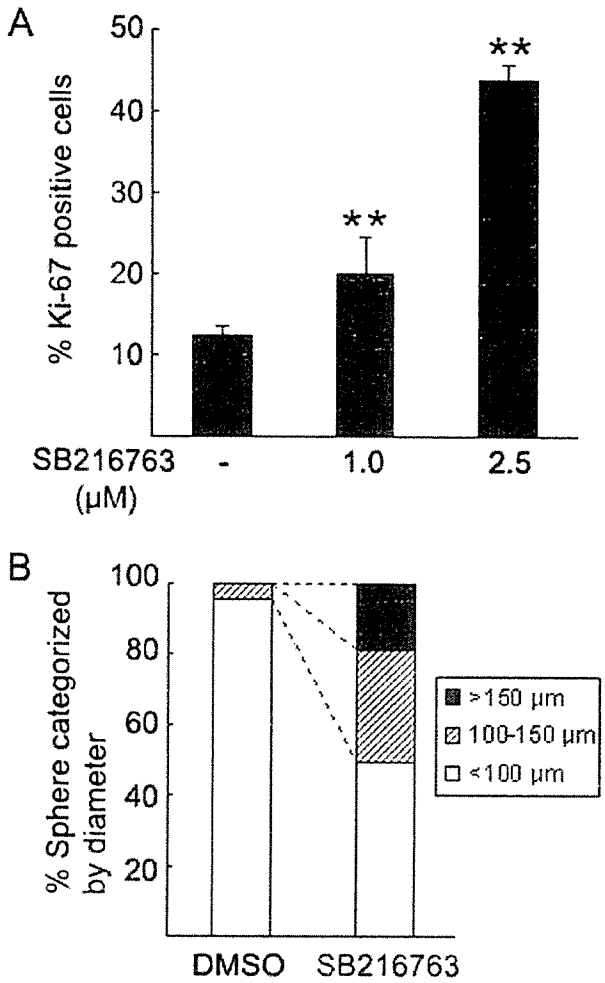

Figure 6. Increase in cell proliferation induced by SB216763 (a GSK3 inhibitor). **(A):** The percentage of Ki-67–positive cells was examined over the same time course described in the legend for Figure 2. The primary spheres were triturated and cultured in the adherent condition with SB216763 for 48 hours. Addition of 2.5 μM SB216763 increases the Ki-67-positive cells to 45% of the total cells. The results are the means ± standard deviations of three replicates. $^{**}p < 0.01$ compared to control cultures. **(B)** The percentages of the spheres were categorized by their diameter as described in the legend for Figure 3. A large proportion of spheres in the culture containing 2.5 μM SB216763 have diameters greater than 100 μm, whereas most spheres in the dimethylsulfoxide (DMSO)-treated control culture have diameters of 100 μm or less. The results are representative of three replicate experiments. The percentages of sphere-forming cells with DMSO and SB216763 were 0.098% ± 0.02% and 0.10% ± 0.01%, respectively.

Cooperative Effect of FGF and Wnt Signaling

Adult retinal stem cells from the ciliary margin have been reported to release a small amount of endogenous FGF2 that promotes sphere formation since antibodies to FGF2 caused a reduction in the number of spheres [9]. To explore the effect of FGF2 on the canonical Wnt pathway, we used SU5402, a small inhibitory molecule that is widely used to specifically interfere with signaling downstream of the FGF receptor (FGFR) [28]. Addition of FGF2 at 10 ng/ml to sphere-derived cell cultures increased the Ki-67–positive cells by threefold, and this activity was reduced to the control level by 6.0 μg/ml SU5402 (Fig. 7A). SU5402 decreased Ki-67–positive cells even in the absence of exogenous FGF2, supporting that endogenous FGF2 signaling was involved in the proliferation of retinal stem cells.

We then added the FGFR inhibitor (SU5402) or FGF2 to the sphere-derived cell cultures in the presence of the GSK3 inhibitor (SB216763) and assessed the number of Ki-67–positive cells. Under all of the above conditions, there was no difference in the cell death estimated by immunocytochemical detection of activated caspase-3 (data not shown). Interestingly, the FGFR inhibitor attenuated the effect of the GSK3 inhibitor on cell proliferation and reduced the number of Ki-67–positive cells from 44%–18% (Fig. 7B). In contrast, exogenous FGF2 enhanced the proliferative effect of the GSK3 inhibitor and increased the Ki-67–positive cells to nearly 80% of the total cells, suggesting that there is an intense cooperative effect of FGF2 and Wnt signaling on cell proliferation of adult retinal sphere-derived cells.

Discussion

In the present study, we showed that Wnt3a increased the number of secondary spheres (promoting self-renewal) and that the expanded cells in the presence of Wnt3a preserved their stem cell abilities to yield differentiated progeny (maintaining multipotency), indicating that Wnt signaling has a mitogenic effect on adult retinal stem cells. It should be noted that sphere-derived cells may include retinal stem cells and committed retinal progenitor cells. Therefore, we refer to the sphere-derived cells as retinal stem/progenitor cells hereafter in this report. Wnt3a induced nuclear accumulation of β-catenin in retinal stem/progenitor cells. More strikingly, the GSK3 inhibitor SB216763, which can activate the canonical Wnt pathway, mimicked Wnt3a activity in terms of the enhancement of retinal stem/progenitor cell proliferation. These findings indicate that the canonical Wnt pathway contributes to the proliferative effect of Wnt3a on retinal stem/progenitor cells. Thus, our study provides evidence that activation of canonical Wnt signaling is useful for expanding retinal stem/progenitor cell pools in vitro. SB216763 is a less-expensive material than recombinant Wnt3a protein and could therefore reduce the cost of tissue engineering. Although the effect of another collateral pathway cannot be excluded, there is little evidence that noncanonical Wnt pathways positively regulate the cell cycle [11]. Although expression of Wnt3a was not detected in murine or avian eye [29, 30], we used commercially available recombinant Wnt3a to activate canonical Wnt pathway in this study. Recombinant Wnt3a was proved to induce self-renewal of hematopoietic stem cells by

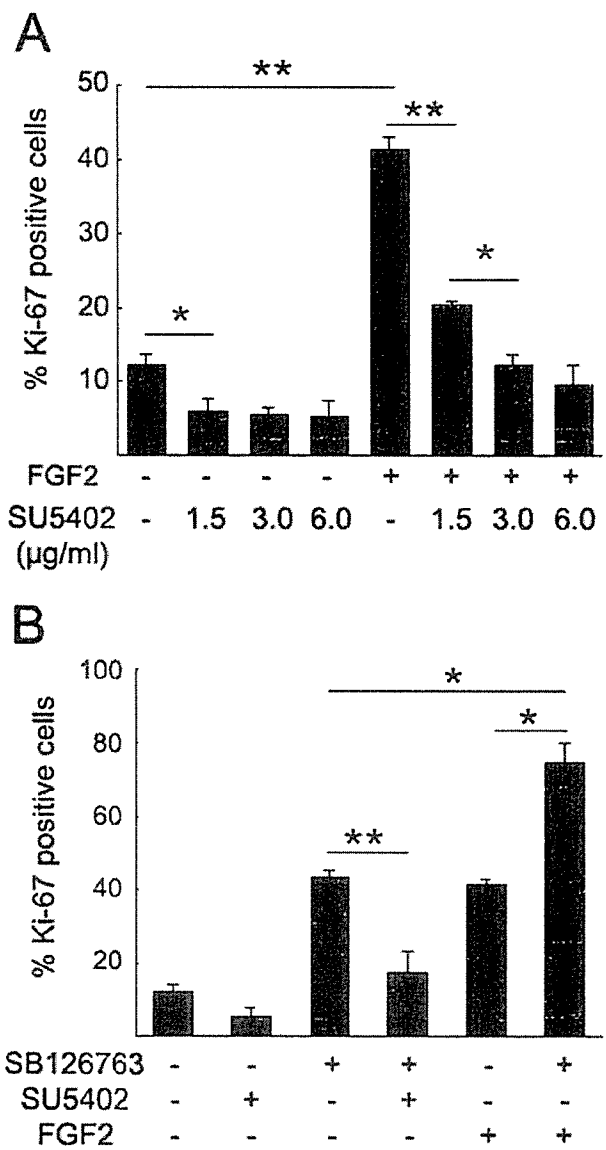

Figure 7. Effects of fibroblast growth factor 2 (FGF2) and its inhibitor on cell proliferation. The percentage of cells expressing Ki-67 was determined as described in the legend for Figure 2. Triturated sphere cells were cultured with FGF2, SU5402 (a FGF receptor inhibitor), SB216763, or their combination for 48 hours. **(A):** In the presence of exogenous FGF2, SU5402 decreases the Ki-67–positive cells in a dose-dependent manner. SU5402 decreases the Ki-67–positive cells, even in the absence of exogenous FGF2, suggesting the existence of endogenous FGF in the sphere-derived cell culture. **(B):** The effect of SB216763 on the cell proliferation is attenuated by SU5402 and enhanced by FGF2. The results are the means ± standard deviations of three replicates. $*p < .05$, $**p < .01$.

activation of canonical Wnt pathway [15], and activation of this pathway promotes proliferation of embryonic chick immature retinal cells [18].

Our study further suggests that the combination of FGF2 and Wnt3a has a strong additive effect on proliferation of adult retinal stem/progenitor cells. In the absence of endogenous FGF signaling, 7% of the total cells were Ki-67–positive. In the presence of the GSK3 inhibitor but without FGF signaling (after addition of the FGF receptor inhibitor), 18% of the total cells were Ki-67–positive (Fig. 7B). If the FGF-responsive and Wnt-responsive cells represent two different populations, 25% (7% + 18%) of the total cells should have been Ki-67–positive after the addition of the GSK3 inhibitor by itself. However, 44% of the cells were Ki67-positive, suggesting synergistic interaction between the FGF and Wnt signaling pathways. In other words, some of the retinal stem/progenitor cells showed cell cycle progression by activation of the canonical Wnt pathway that was dependent on endogenous FGF signaling. Concurrently with our present results, which we presented in the recent annual meeting of the Association for Research in Vision and Ophthalmology [31], Das et al. independently showed that Wnt3a increased the number of primary spheres derived from an adult ciliary margin in the presence of FGF2 [32], supporting our data.

As demonstrated in this study, the adult murine ciliary margin contains Wnt signal-responsive stem cells, although they are mitotically quiescent in vivo [33–36]. In addition, Wnt2b was reported to be expressed in the adult murine neural retina [29] and had the potential to induce proliferation of developing chick retinal precursors in vitro and in vivo via the canonical pathway [18]. The mechanism responsible for this difference between the in vivo and in vitro conditions remains unknown. N- and P-cadherin are expressed in the adult ciliary epithelium [37] and may contribute to attenuate cell proliferation by interference of the relocation of β-catenin into the nucleus (reviewed by Nelson et al. [38]). Secreted Wnt inhibitors, such as Sfrp family members expressed in the adult murine retina [29], also cannot be excluded because the roles of these molecules in the retina have not been well clarified. Another possibility is signal crosstalk with some other pathways, such as FGF signaling. The decreased FGF2 expression in the growing retina [39] could diminish the FGF-dependent proliferative effect of Wnt signaling. However, FGF2 may not actually be the partner of Wnt signaling in vivo because injured retinas were reported to express FGF2 but retinal regeneration by proliferation of retinal stem cells was not observed [40–43].

How can Wnt signaling be applied to stem cell therapy? It was recently reported that sphere cells generated from the ciliary margin could be incorporated into damaged or developing retinas, where they expressed retinal cell–specific markers, such as rhodopsin, syntaxin, and protein kinase C [44, 45]. Wnt signaling must be valuable for increasing the number of sphere colonies by continuous subcloning. Recently, Moshiri and Reh [46] reported that postnatal murine retinal margin cells showed a limited potential to regenerate retinal neurons using *patched* $(ptc)^{+/-}$ mice, in which Sonic hedgehog signaling is partially

activated. In $ptc^{+/-}$ mice bred onto a retinal degeneration background, newly generated neurons and photoreceptors were observed at the retinal margin in vivo, similar to that in lower vertebrates. This observation suggests the possibility that targeted manipulation of stem cells in the ciliary margin may lead to regeneration of damaged retinal neurons in higher vertebrates. If this is the case, the present results indicate that some molecules involved in the canonical Wnt pathway may be therapeutic targets. The effect of Wnt3a on the differentiation of the retinal stem cells derived from adult ciliary margin is not yet well clarified, and little is known about the crosstalk of Wnt signaling with the other mitotic factors for ciliary margin cells, such as insulin-like growth factor [47]. Further studies are required to fully characterize the proliferation and differentiation of retinal stem cells.

CONCLUSION

Wnt3a increased the self-renewal of retinal stem cells from the adult ciliary margin via the canonical pathway. A GSK3 inhibitor could mimic the proliferative effect of Wnt3a, which was partly dependent on FGF signaling. FGF and Wnt signaling showed a synergistic effect on retinal stem/progenitor cell proliferation, stimulating more than 75% of the total cells to become Ki-67–positive proliferating cells. These results may provide a novel therapeutic strategy for in vitro pooling or in vivo activation of retinal stem cells derived from the adult ciliary margin.

ACKNOWLEDGMENTS

The authors are very grateful to M. Ohta-Teramoto for secretarial assistance and to Y. Saiki for technical help. This work was supported by a Grant-in-Aid for 21st Century COE Research "Cell Fate Regulation Research and Education Unit" and Grant-in-Aid for Scientific Research (B) from the Ministry of Education, Culture, Sports, Science and Technology.

DISCLOSURES

The authors indicate no potential conflicts of interest.

REFERENCES

1 Perron M, Kanekar S, Vetter ML et al. The genetic sequence of retinal development in the ciliary margin of the Xenopus eye. Dev Biol 1998; 199:185–200.

2 Wetts R, Serbedzija GN, Fraser SE. Cell lineage analysis reveals multipotent precursors in the ciliary margin of the frog retina. Dev Biol 1989;136:254–263.

3 Beach DH, Jacobson M. Patterns of cell proliferation in the retina of the clawed frog during development. J Comp Neurol 1979;183:603–613.

4 Meyer RL. Evidence from thymidine labeling for continuing growth of retina and tectum in juvenile goldfish. Exp Neurol 1978;59:99–111.

5 Johns PR. Growth of the adult goldfish eye, III: source of the new retinal cells. J Comp Neurol 1977;76:343–357.

6 Straznicky K, Gaze RM. The growth of the retina in Xenopus laevis: an autoradiographic study. J Embryol Exp Morphol 1971;26:67–79.

7 Hollyfield JG. Differential addition of cells to the retina in Rana pipiens tadpoles. Dev Biol 1968;18:163–179.

8 Ahmad I, Tang L, Pham H. Identification of neural progenitors in the adult mammalian eye. Biochem Biophys Res Commun 2000;270:517–521.

9 Tropepe V, Coles BL, Chiasson BJ et al. Retinal stem cells in the adult mammalian eye. Science 2000;287:2032–2036.

10 Engelhardt M, Wachs FP, Couillard-Despres S et al. The neurogenic competence of progenitors from the postnatal rat retina in vitro. Exp Eye Res 2004;78:1025–1036.

11 Pandur P, Maurus D, Kuhl M. Increasingly complex: new players enter the Wnt signaling network. Bioessays 2002;24:881–884.

12 Willert K, Nusse R. Beta-catenin: a key mediator of Wnt signaling. Curr Opin Genet Dev 1998;8:95–102.

13 van de Wetering M, Sancho E, Verweij C et al. The beta-catenin/TCF-4 complex imposes a crypt progenitor phenotype on colorectal cancer cells. Cell 2002;111:241–250.

14 Reya T, Duncan AW, Ailles L et al. A role for Wnt signalling in self-renewal of haematopoietic stem cells. Nature 2003;423:409–414.

15 Willert K, Brown JD, Danenberg E et al. Wnt proteins are lipid-modified and can act as stem cell growth factors. Nature 2003;423:448–452.

16 Liu BY, McDermott SP, Khwaja SS et al. The transforming activity of Wnt effectors correlates with their ability to induce the accumulation of mammary progenitor cells. Proc Natl Acad Sci U S A 2004;101:4158–4163.

17 Sato N, Meijer L, Skaltsounis L et al. Maintenance of pluripotency in human and mouse embryonic stem cells through activation of Wnt signaling by a pharmacological GSK-3-specific inhibitor. Nat Med 2004; 10:55–63.

18 Kubo F, Takeichi M, Nakagawa S. Wnt2b controls retinal cell differentiation at the ciliary marginal zone. Development 2003;130:587–598.

19 Hsieh M, Johnson MA, Greenberg NM et al. Regulated expression of Wnts and Frizzleds at specific stages of follicular development in the rodent ovary. Endocrinology 2002;143:898–908.

20 Heller RS, Dichmann DS, Jensen J et al. Expression patterns of Wnts, Frizzleds, sFRPs, and misexpression in transgenic mice suggesting a role for Wnts in pancreas and foregut pattern formation. Dev Dyn 2002;225: 260–270.

21 Tulac S, Nayak NR, Kao LC et al. Identification, characterization, and regulation of the canonical Wnt signaling pathway in human endometrium. J Clin Endocrinol Metab 2003;88:3860–3866.

22 Hoang BH, Kubo T, Healey JH et al. Expression of LDL receptor-related protein 5 (LRP5) as a novel marker for disease progression in high-grade osteosarcoma. Int J Cancer 2004;109:106–111.

23 Kee N, Sivalingam S, Boonstra R et al. The utility of Ki-67 and BrdU as proliferative markers of adult neurogenesis. J Neurosci Methods 2002; 115:97–105.

24 Hsieh JC, Rattner A, Smallwood PM et al. Biochemical characterization of Wnt-frizzled interactions using a soluble, biologically active vertebrate Wnt protein. Proc Natl Acad Sci U S A 1999;963546–3551.

25 Dann CE, Hsieh JC, Rattner A et al. Insights into Wnt binding and signalling from the structures of two Frizzled cysteine-rich domains. Nature 2001;412:86–90.

26 Cross DA, Culbert AA, Chalmers KA et al. Selective small-molecule inhibitors of glycogen synthase kinase-3 activity protect primary neurones from death. J Neurochem 2001;77:94–102.

27 Doble BW, Woodgett JR. GSK-3: tricks of the trade for a multi-tasking kinase. J Cell Sci 2003;116:1175–1186.

28 Mohammadi M, McMahon G, Sun L et al. Structures of the tyrosine kinase domain of fibroblast growth factor receptor in complex with inhibitors. Science 1997;276:955–960.

29 Liu H, Mohamed O, Dufort D et al. Characterization of Wnt signaling components and activation of the Wnt canonical pathway in the murine retina. Dev Dyn 2003;227:323–334.

30 Jin EJ, Burrus LW, Erickson CA. The expression patterns of Wnts and their antagonists during avian eye development. Mech Dev 2002;116: 173–176.

31 Inoue T, Fukushima M, Kagawa T et al. Wnt3a promotes proliferation of retinal stem cells. IOVS 2004;45:ARVO E-Abstract 5386.

32 Das AV, James J, Magana-Arachchi DN et al. Wnt signaling regulates ocular neural stem cells. IOVS 2004;45:ARVO E-Abstract 5396.

33 Cepko CL, Austin CP, Yang X et al. Cell fate determination in the vertebrate retina. Proc Natl Acad Sci U S A 1996;93:589–595.

34 Pittack C, Grunwald GB, Reh TA. Fibroblast growth factors are necessary for neural retina but not pigmented epithelium differentiation in chick embryos. Development 1997;124:805–816.

35 Feijen A, Goumans MJ, van den Eijnden-van Raaij AJ. Expression of activin subunits, activin receptors and follistatin in postimplantation mouse embryos suggests specific developmental functions for different activins. Development 1994;120:3621–3637.

36 Bodenstein L, Sidman RL. Growth and development of the mouse retinal pigment epithelium, I: cell and tissue morphometrics and topography of mitotic activity. Dev Biol 1987;121:192–204.

37 Xu L, Overbeek PA, Reneker LW. Systematic analysis of E-, N- and P-cadherin expression in mouse eye development. Exp Eye Res 2002;74: 753–760.

38 Nelson WJ, Nusse R. Convergence of Wnt, beta-catenin, and cadherin pathways. Science 2004;303:1483–1487.

39 Gao H, Hollyfield JG. Basic fibroblast growth factor in retinal development: differential levels of FGF2 expression and content in normal and retinal degeneration (rd) mutant mice. Dev Biol 1995;169:168–184.

40 Casson RJ, Chidlow G, Wood JP et al. The effect of retinal ganglion cell injury on light-induced photoreceptor degeneration. Invest Ophthalmol Vis Sci 2004;45:685–693.

41 Miyashiro M, Ogata N, Takahashi K et al. Expression of basic fibroblast growth factor and its receptor mRNA in retinal tissue following ischemic injury in the rat. Graefes Arch Clin Exp Ophthalmol 1998;236:295–300.

42 Cao W, Wen R, Li F et al. Mechanical injury increases bFGF and CNTF mRNA expression in the mouse retina. Exp Eye Res 1997;65:241–248.

43 Wen R, Song Y, Cheng T et al. Injury-induced upregulation of bFGF and CNTF mRNAS in the rat retina. J Neurosci 1995;15:7377–7385.

44 Chacko DM, Das AV, Zhao X et al. Transplantation of ocular stem cells: the role of injury in incorporation and differentiation of grafted cells in the retina. Vision Res 2003;43:937–946.

45 Coles BL, Angenieux B, Inoue T et al. Facile isolation and the characterization of human retinal stem cells. Proc Natl Acad Sci U S A 2004;101:15772–15777.

46 Moshiri A, Reh TA. Persistent progenitors at the retinal margin of ptc$^{+/-}$ mice. J Neurosci 2004;24:229–237.

47 Fischer AJ, Reh TA. Identification of a proliferating marginal zone of retinal progenitors in postnatal chickens. Dev Biol 2000;220:197–210.

Available online at www.sciencedirect.com
SCIENCE DIRECT
ELSEVIER
Experimental Eye Research 82 (2006) 362–370
EXPERIMENTAL EYE RESEARCH
www.elsevier.com/locate/yexer

Rho-associated protein kinase inhibitor, Y-27632, induces alterations in adhesion, contraction and motility in cultured human trabecular meshwork cells

Tomoyo Koga[a], Takahisa Koga[a], Maiko Awai[a], Jun-ichiro Tsutsui[a], Beatrice Y.J.T. Yue[b], Hidenobu Tanihara[a,*]

[a]*Department of Ophthalmology & Visual Science, Kumamoto University Graduate School of Medical Sciences, Honjo 1-1-1, Kumamoto 860-8556, Japan*
[b]*Department of Ophthalmology and Visual Sciences, University of Illinois at Chicago, College of Medicine, USA*

Received 28 March 2005; accepted in revised form 11 July 2005
Available online 25 August 2005

Abstract

We investigated the roles of Rho-associated protein kinase (ROCK) in regulating activities such as adhesion, contraction and migration in cultured human trabecular meshwork (TM) cells. Human TM cells in culture were treated with Y-27632, a specific ROCK inhibitor. Trypan blue exclusion test and TUNEL staining showed little or no direct toxicity of Y-27632 on TM cells. By MTT assay, Y-27632 did not significantly affect the proliferation of TM cells. The cell adhesion assay showed that Y-27632 promoted the cell adhesiveness to both fibronectin and collagen type I in a dose-dependent manner. Collagen gel contraction activity of TM cells was significantly inhibited by the treatment of Y-27632 in a dose-dependent manner. The addition of Y-27632 accelerated motility of TM cells in wound healing assay. Phosphorylated LIM kinase 2 and cofilin, related to actin bundling and integrin clustering, were dephosphorylated (activated) by Y-27632. In conclusion, Y-27632 elicits profound effects on TM cell activities including adhesion, gel contraction, and cell motility. These Y-27632-induced changes of TM cells may be relevance to the physiology of the aqueous outflow system.

Keywords: Rho; ROCK; Y-27632; trabecular meshwork cells

1. Introduction

In human eyes, a majority (83–96%) of the aqueous humour leaves the eye through the trabecular meshwork (TM) and Schlemm's canal (conventional outflow) under physiologic conditions (Jocson and Sears, 1971; Bill and Phillips, 1971). Accumulating data have suggested that TM cells and their extracellular matrix (ECM) play important roles in regulating the conventional outflow pathway and the intraocular pressure (IOP). For instance, with aging, the aqueous outflow resistance increases while the number of TM cells decreases and the ECM composition in the juxtacanalicular region changes (Alvarado et al., 1981; McMenamin et al., 1986; Miyazaki et al., 1987). Fewer TM cells and abnormal deposition of the ECM have also been reported in glaucomatous eyes compared with normal eyes (Rohen, 1983; Alvarado et al., 1984; Alvarado et al., 1986; Knepper et al., 1996). It is believed that the outflow facility can be improved by modulating the TM cellular behaviour and that new IOP-lowering drugs may be designed through this process. So far, it has been reported that IOP can be reduced by cytoskeletal drugs such as cytochalasins (Kaufman and Barany, 1977; Kaufman and Erickson, 1982), ethacrynic acid (Epstein et al., 1987), a serine-threonine kinase inhibitor H-7 (Tian et al., 1998; Epstein et al., 1999), and protein kinase C inhibitor (Khurana et al., 2003).

Rho guanosine triphosphatase (GTPase), a member of the Rho subgroups of the Ras superfamily, participates in signalling pathways that play key roles in formation of actin stress fibres and focal adhesions, cytoskeletal rearrangements, cell morphology, cell motility and smooth muscle

Abbreviations effects of Y-27632 on human trabecular meshwork cells.

* Corresponding author. Hidenobu Tanihara, Department of Ophthalmology & Visual Science, Kumamoto University Graduate School of Medical Sciences, Honjo 1-1-1, Kumamoto 860-8556, Japan
E-mail address: tanihara@pearl.ocn.ne.jp (H. Tanihara).

0014-4835/$ - see front matter © 2005 Elsevier Ltd. All rights reserved.
doi:10.1016/j.exer.2005.07.006

contraction (Takai et al., 1995; Nobes and Hall, 1995; Kaibuchi et al., 1999). Recently, several putative target molecules of Rho have been identified as Rho effectors, including Rho-associated coiled coil-forming protein kinase named ROCK I (Nakagawa et al., 1996) (also known as p160 ROCK (Ishizaki et al., 1996)), and its isoform, ROCK II (Nakagawa et al., 1996) (also known as Rho kinase (Matsui et al., 1996) and ROK α (Leung et al., 1995)). ROCKs are important factors regulating focal adhesions and stress fibre formation in cultured fibroblasts and epithelial cells (Riento and Ridley, 2003). Y-27632 has been identified as a specific inhibitor of the ROCK/ROK family of protein kinases (Uehata et al., 1997). In a previous report from our laboratory, we noted that administration of this compound resulted in a significant reduction of IOP in rabbits in a dose-dependent manner (Honjo et al., 2001). We also demonstrated the presence of p160 ROCK in human TM cells and showed that ROCK inhibitors altered cell shape, disrupted actin bundles, and impaired focal adhesion formation (Honjo et al., 2001). Our studies along with others suggested that alterations in TM cellular behaviours might be the basis for the observed changes in the outflow facility (Tian et al., 2000; Lutjen-Drecoll et al., 2001; Rao et al., 2001).

Herein, we extended our effort in elucidating the physiology of the aqueous humour outflow by examining further the effects of Y-27632 on activities, including viability, proliferation, adhesion on the ECM, collagen gel contraction and motility of human TM cells in culture.

2. Materials and methods

2.1. Culture of human TM cells

Human eyes from donors aged 15, 22 and 47 years were obtained from the Illinois Eye Bank (Chicago). The procurement of tissues was approved by the Institutional Review Board at the University of Illinois at Chicago in compliance with the declaration of Helsinki. Trabecular tissues excised from eyes were cultured on Falcon Primaria flasks (Becton Dickson, Lincoln Park, NJ), as previously described (Yue et al., 1990; Sawaguchi et al., 1992; Zhou et al., 1996; Choi et al., 2005). The culture medium included Dulbecco's modified Eagle's medium (DMEM), 10% fetal bovine serum (FBS), and antibiotics. Cells were maintained at 37 °C in a 95% air −5% CO_2 incubator, and passaged using the trypsin-EDTA method. Human TM cells from passages 3 through 8 were used for subsequent studies.

2.2. Trypan blue exclusion test

The cytotoxicity of Y-27632 was evaluated using the trypan blue exclusion test. Viable cells were counted in vitro according to a previously described method (Jain et al., 1992). Briefly, 5×10^5 human TM cells were plated onto 100-mm dishes and grown for 24 hr. The medium was then replaced with fresh medium without or with Y-27632 (1, 10 and 100 μM). Twenty-four hour after the treatment, the cells were trypsinized and 1 mL of cell suspension containing 2×10^6 TM cells was prepared; 50 μL of 0.1% (vol/vol) trypan blue solution was then added to the cell suspension. Stained and unstained cells were counted by hemacytometer under a microscope 3 min after trypan blue treatment. The percentage of cell viability was calculated using the following formula: % cell viability=(viable cell count/total cell count)×100. Five independent experiments were performed.

2.3. Terminal deoxyribonucleotidyl transferase (TdT)-mediated fluroscein-16-dUTP nick end-labelling (TUNEL) assay

Human TM cells plated on glass coverslips in 12-well culture plates were grown at 37 °C for 24 hr. Y-27632 (10 and 100 μM) was added and incubated for an additional 24 hr. The cells were then fixed with 4% paraformaldehyde in phosphate-buffered saline (PBS) for 15 min, washed with PBS, and permeabilized with 0.2% Triton X-100 for 5 min. For positive controls, the cells were incubated with 1 unit mL^{-1} DNase I (Invitrogen, Carlsbad, CA) for 10 min. TUNEL reaction was performed with Apoptosis Detection System, Fluorescein (Promega, Madison, WI) at 37 °C for 60 min according to the manufacture's protocol. After mounting using an anti-fade kit (Molecular Probes, Eugene, OR), the staining was observed under a fluorescence microscope (IX71, Olympus, Tokyo, Japan).

2.4. Cell proliferation assay

Proliferation of cultured human TM cells was measured by 3, (4,5-dimethyl-2-thiazolyl)-2,5-diphenylate-2Htetrazolium bromide (MTT), using a commercially available kit (Nacalai Tesque, Kyoto, Japan). Cells were plated in culture medium at a density of 1×10^4 cells per well in 96-well plates and allowed to adhere for 24 hr. After washing, the cultures were fed with fresh media, without or with Y-27632 (1, 10 and 100 μM) for 72 hr, and finally treated with 5 mg mL^{-1} MTT for 4 hr at 37 °C. The MTT solution was aspirated, and the formazan crystals were dissolved in detergent reagent for 10 min. The relative cell number was determined based on the optical absorbance of the formazan at 570 nm, using a control wavelength of 655 nm measured in automatic plate reader (BioRad, Hercules, CA).

2.5. Cell adhesion assay

Cell adhesion assay was conducted as previously described (Zhou et al., 1996). For the assay, the wells of 96-well plates were coated overnight with fibronectin (10 μg mL^{-1}) (Sigma, St. Louis, MO) or collagen type I (0.5 μg mL^{-1}) (Calbiochem, San Diego, CA) at 4 °C.

The remaining binding sites were blocked by 0.1% of bovine serum albumin (BSA) in PBS for 2 hr at room temperature. Human TM cells were suspended in culture medium containing 2 mg mL^{-1} of BSA without or with Y-27632 (at 10 or 100 μM), and were loaded ($n=4$) onto coated wells at 8×10^4 cells per well. After incubation for 60 min, the unattached cells were removed by aspiration. The remaining cells were fixed in 10% formalin and stained with 1% toluidine blue. They were then lysed and the intensity of the blue stain was measured with a microplate reader at 600 nm as an indication of cell density.

2.6. Immunocytochemical studies

TM cells were plated on glass coverslips in culture medium, and cultured overnight. Y-27632 at 100 μM was added for 60 min. After the drug exposure, the cells were fixed and permeabilized for 2 min in 3% paraformaldehyde-PBS with 5% Triton X-100 (Wako, Osaka, Japan), and were further fixed for 20 min with 3% paraformaldehyde. The samples were blocked in 2% BSA for 30 min. The coverslips were incubated for 60 min at room temperature with anti-β-catenin antibody (Sigma) diluted at 1:2000, or anti-pan-cadherin antibody (Abcam, Cambridgeshire, UK) diluted at 1:500 with blocking solutions. The samples were washed 3 times with PBS and incubated with Cy-3 conjugated anti-mouse secondary antibody (Jackson ImmunoResearch, West Grove, PA) or FITC conjugated anti-mouse secondary antibody (Jackson ImmunoResearch) for 30 min. After washing, the cells were mounted with anti-fade and observed by fluorescence microscope IX71.

2.7. Immunoblot analysis

Human TM cells (2×10^5 cells per well) were plated overnight in 6-well Falcon plates and were incubated with 10 or 100 μM of Y-27632 for 0.5 or 1 hr. Immediately after Y-27632 incubation or following a recovery period of 2 hr, the cells were gently washed with PBS and lysed in 500 μL of NuPAGE LDS sample buffer (Invitrogen) containing 0.05 M DTT (Invitrogen). The NuPAGE LDS sample buffer was commercially available, and consisted of 109 M Glycerol, 140.5 mM Tris, 106 mM Tris–HCl, 73 mM Lithium Dodesyl Sulfate, and 0.51 mM EDTA. After heating at 70 °C for 10 min in sample buffer, 15 μL of each sample was subjected to 4–12% NuPAGE Bis-Tris gel (Invitrogen) or 4–20% Tris-Glycine gel (Invitrogen) electrophoresis and transferred to nitrocellulose membrane (Protran, Schleicher and Schuell Bioscience, Keene, NH). The membrane was blocked for 60 min at room temperature in 5% skim milk and 0.1% Tween-20 diluted in Tris-buffered saline (TTBS) to minimize nonspecific immunoreaction. Some membranes were incubated for 1 hr at room temperature with anti-β-catenin antibody diluted at 1:4000, anti-pan-cadherin antibody diluted at 1:1000, anti-β-actin antibody (Ambion, Austin, TX) diluted at 1:500, or anti-glyceraldehyde 3-phosphate dehydrogenase (GAPDH) antibody (Biogenesis laboratories, Kommetjie, South Africa) diluted at 1:200 with dilution buffer (5% BSA in TTBS). Other membranes were subsequently incubated overnight at 4 °C with anti-phospho-LIM kinase 1/2 (Cell Signalling), anti-cofilin (Cell Signalling) or anti-phospho-cofilin (Cell Signalling) antibody diluted at 1:1000 with dilution buffer. The membrane was washed three times at room temperature for 10 min with TTBS. It was then incubated for 30 min at room temperature with horseradish-peroxidase-conjugated anti-mouse IgG antibody (1:500, Amersham Biosciences, Buckinghamshire, UK). After further washing, the membranes were incubated with enhanced chemiluminescence (Amersham Biosciences) and exposed to autoradiogram film to visualize immunoreactive bands.

2.8. Gel contraction assay

Collagen gel contraction assay was performed as previously described (Nakamura et al., 2002; Nakamura et al., 2003), with minor modifications. The wells of 24-well culture clusters were each coated at 37 °C with 1% BSA for 1 hr. Human TM cells were trypsinized and resuspended in culture medium at a density of 2.2×10^6 cells mL^{-1} without or with Y-27632 (1, 10 and 100 μM). Collagen type I (Nitta-gelatin, Osaka, Japan), 10×DMEM, reconstitution buffer (Nitta-gelatin), TM cell suspension and water were mixed in an ice bath at a ratio of 7:1:1:1:1 (final concentration of collagen type I, 1.9 mg mL^{-1}; final cell density, 2×10^5 cells mL^{-1}). The resultant mixture (0.5 mL) was added to each well of the BSA coated culture clusters, and collagen gel formation was induced by incubation at 37 °C for 90 min. DMEM (0.5 mL), without or with Y-27632 (1, 10 and 100 μM), was then added on top of the collagen gels. After 1 hr, the gels were freed from the walls of the culture wells with the use of a micro spatula. The diameter of the collagen gels was scanned into a computer and measured with a ruler every 24 hr for 3 days. The extent of contraction of the collagen gels mediated by the TM cells was expressed as decrease in gel diameter compared with the initial diameter.

2.9. Measurements of wound healing (cell motility) activities

Human TM cells were grown to confluence in 100-mm tissue culture dishes. Three or four sites in each dish were scraped from the confluent cells with a yellow plastic pipette tip to create a cleared line. The medium was removed and replaced with fresh medium without or with Y-27632 (10 and 100 μM). After incubation at 37 °C for 9 hr, the progress of cells moving into the wound area was photographed by microscope digital camera, DP70 (Olympus) and loaded into computer software, DP controller (Olympus). The shortest distance between the

edges of migrated TM cells (including its' protrusions) from both sides was measured by the ruler of this computer soft.

2.10. Stastical analysis

Data are presented as the mean ± S.D. and were statistically analysed by Student's *t*-test.

3. Results

3.1. Toxicologic experiments of Y-27632 on human TM cells

Trypan-blue exclusion test was performed to determine whether Y-27632 was toxic to TM cells. The percentage of the living TM cells without trypan blue staining was 99.7 ± 0.4% in control cultures without Y-27632 treatments ($n=5$). In experimental cultures treated with various concentrations of Y-27632, the percentages of trypan blue free (living) cells were between 99.4 and 99.6% ($n=5$), not statistically significant different from that in controls (Table 1). TUNEL staining was performed to investigate directly the effect on human TM cell death by the addition of Y27632. After treatments with DNase I, almost all of the TM cells became TUNEL-positive (Fig. 1). On the other hand, no TUNEL-positive cells could be detected even after 24 hr of Y-27632 treatment, although typical morphological changes were evident by light microscopy. Effects of Y-27632 on proliferation in cultured TM cells were evaluated with the use of MTT assay. No statistically significant differences between Y-27632 treated TM cells and controls could be discerned (Fig. 2). This inhibitor thus displayed little cytotoxicity and had no effect on the proliferative activity of TM cells.

3.2. Influence of Y-27632 on adhesion of TM cells onto ECM

To elucidate interactions between cultured human TM cells and ECM components, adhesion of TM cells onto

Table 1
Trypan blue exclusion test to evaluate cytotoxicity of Y27632 on cultured TM cells

	Exp. 1	Exp. 2	Exp. 3	Exp. 4	Exp. 5	Mean ± S.D.
TM (control)	100	100	100	99.2	99.3	99.7 ± 0.4
TM + Y27632 (1 μM)	98.9	99.1	100	100	99.4	99.4 ± 0.5
TM + Y27632 (10 μM)	100	99.1	100	100	98.9	99.6 ± 0.5
TM + Y27632 (100 μM)	99.1	100	100	99.1	100	99.6 ± 0.5

The percent of viable cells are shown. S.D., standard deviation; Exp, experiment.

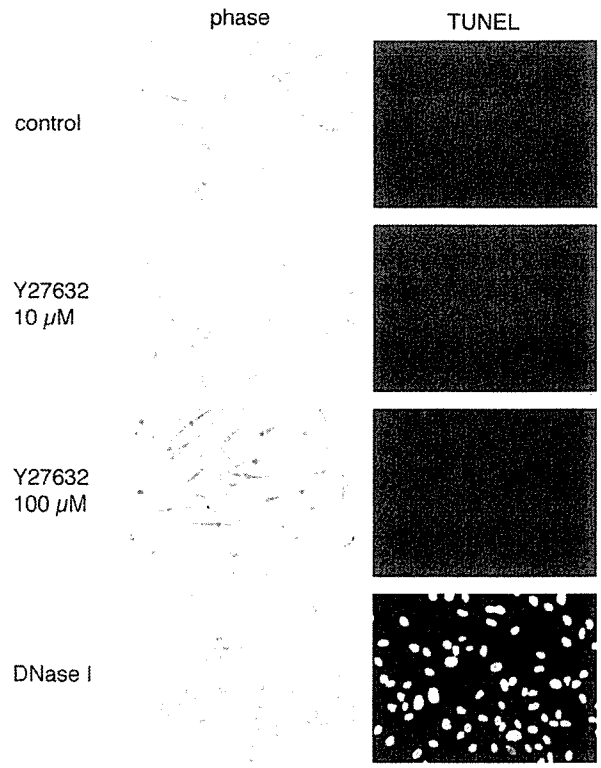

Fig. 1. Terminal deoxyribonucleotidyl transferase (TdT)- mediated fluroscein-16-dUTP nick end-labelling (TUNEL) staining on human TM cells without (control) or with the Y-27632 treatment for 24 hr. TUNEL positive cells were undetectable in TM cultures regardless whether they were untreated or treated with 10 μM or 100 μM Y-27632. In positive controls in which TM cultures were treated with DNase I, almost all of the cells were TUNEL positive (green).

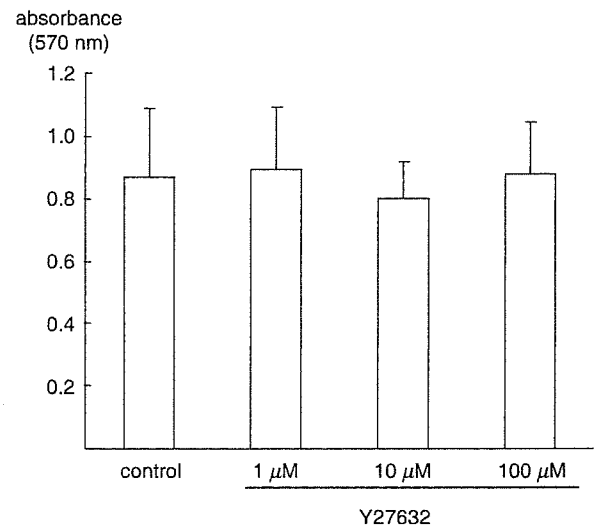

Fig. 2. Effect of Y-27632 on proliferation in human TM cells. Proliferation was measured by 3,(4,5-dimethyl-2-thiazolyl)-2,5-diphenylate-2H-tetrazolium bromide (MTT) assay. The data were expressed as the mean ± S.D. ($n=8$). Y-27632 did not affect human TM cell proliferation at any of concentrations (1, 10 or 100 μM).

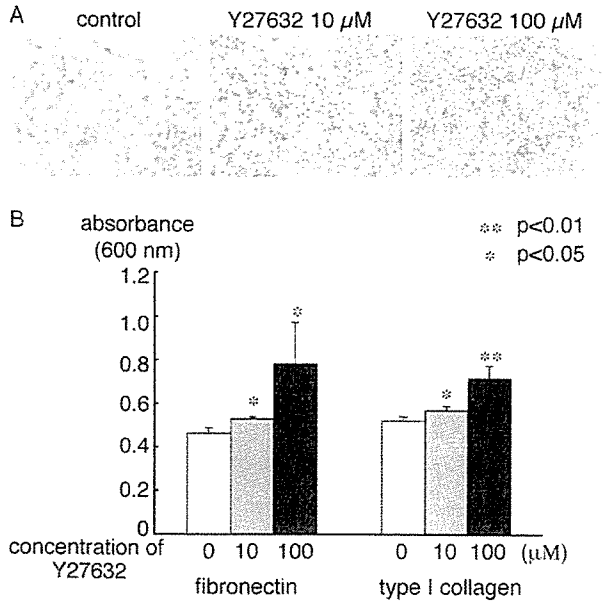

Fig. 3. Effect of Y-27632 on adhesion of human TM cells. Cells were plated on fibronectin (10 μg mL^{-1}) or collagen type I (0.5 μg mL^{-1}), and allowed to adhere in the absence or presence of Y-27632 (10 or 100 μM) for 60 min. The adhered cells were stained with 1% toluidine blue. The stained cells were lysed and the absorbance at 600 nm, a reflection of cell density, was measured. Data expressed as mean ± S.D. ($n=4$) were analysed by Student's t-test. The stained cells that were adhered on fibroectin are shown in A. Quantitative data are shown as bar graphs in B.

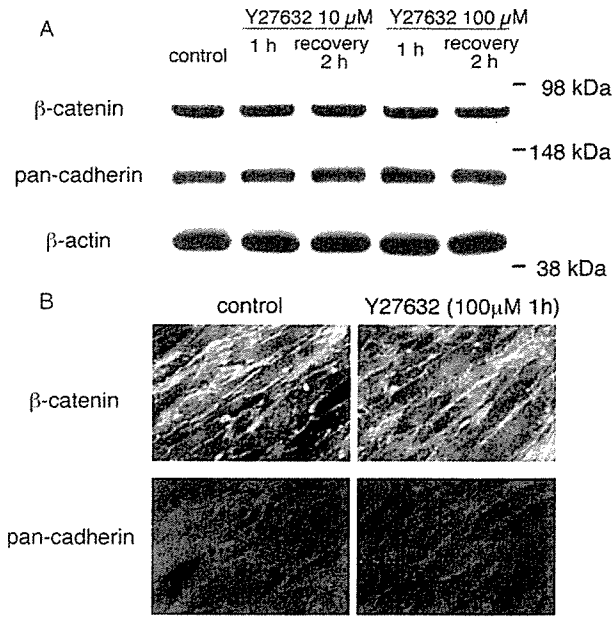

Fig. 4. (A) Level of β-catenin and pan-cadherin proteins in human TM cells treated with 0 (control), 10, or 100 μM of Y-27632. Immunoblot study was performed using lysates of cells collected immediately after Y-27632 treatment for 1 hr, or after incubation with fresh culture media without Y-27632 for an additional 2 hr (recovery 2 hr). (B) Distribution of β-catenin and pan-cadherin in human TM cells 1 hr after exposure to 100 μM of Y-27632. Experiments were repeated 3 times, yielding similar results.

fibronectin-coated or collagen type I-coated dishes was assayed. Compared with controls, a greater number of Y-27632-treated TM cells adhered onto fibronectin. Adhesion of TM cells to collagen type I was also increased by the addition of Y27632. The TM adhesion to both fibronectin and collagen type I was increased with increasing concentrations of Y-27632 (Fig. 3).

3.3. Effect of Y-27632 on cell–cell junction

In immunoblot analysis of cell–cell adhesion molecules, β-catenin (using anti-β-catenin antibody) and cadherins (using anti-pan-cadherin antibody) were detected under control medium without Y27632. These expression levels were not changed after Y27632 treatment for 1 hr and recovery for 2 hr. In immunocytochemical study, under control medium without Y27632, the cell–cell adhesions delineated by β-catenin and cadherins staining appeared as continuous or partially segmented lines along cell borders. After Y27632 treatment, these staining were also detected as continuous or partially segmented lines along borders of packed TM cells (Fig. 4).

3.4. Gel contraction assay

TM cells are known to induce contraction of collagen gel within which they are cultured (Nakamura et al., 2002; Nakamura et al., 2003). In our experiments, 24 hr after plating human TM cells with collagen gels, the change of the diameter of gels from the original value (16 mm) was 6.89 ± 0.38 mm ($n=3$). On the other hand, with 1, 10 and 100 μm Y-27632, the change of collagen gel diameter was 5.8 ± 0.8, 0.2 ± 0.4 and 0 mm (no detectable changes), respectively (Fig. 5). The results were statistically significant ($p<0.001$) and a dose dependency was evident. Similar results were also seen in experiments at 48 and 72 hr time points.

3.5. Wound healing (cell motility) activity of TM cells

Human TM cells in confluent cultures were scraped with a pipet tip to create cell-free wounds. At 9 hr after the scraping, the distance between the edges of exposed region was measured to be 75.0 ± 16.2, 28.1 ± 9.4 and 3.1 ± 5.4%, respectively, with Y-27632 at 0 (control), 10 and 100 μm (Fig. 6). The increase in the wound healing (cell motility) activity by Y-27632 was significant and concentration dependent.

In an effort to elucidate mechanisms related to actin remodelling and migration activities, we studied the status of phosphorylated forms of LIM kinase and cofilin. It has been reported that dephosphorylated LIM kinase leads to the dephosphorylated (active) form of cofilin, resulting in depolymerization of actin filament and promoting actin remodelling (Bamburg, 1999). Our immunoblot analysis showed that Y-27632 decreased the level of both

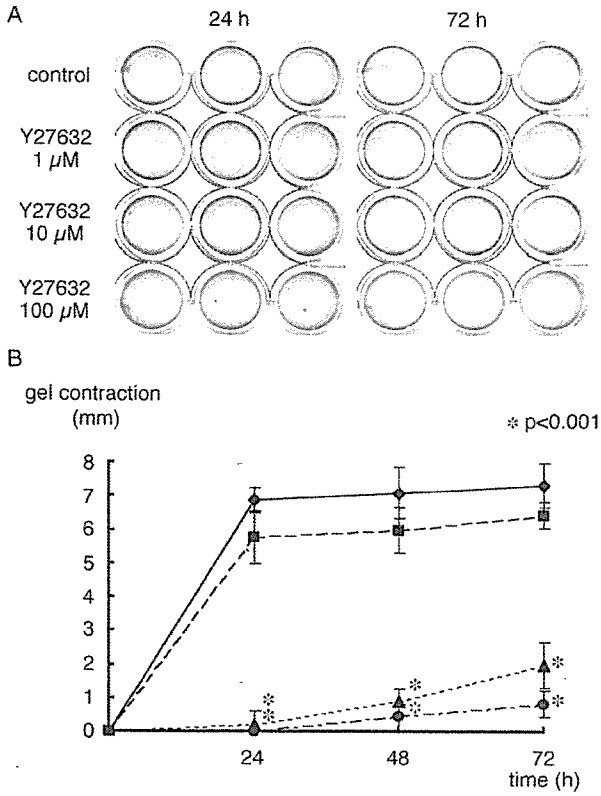

Fig. 5. Effect of Y-27632 on collagen gel contraction by human TM cells. (A) Collagen gels were incubated without (control) or with Y-27632 (1, 10 or 100 μM) for 24 or 72 hr. (B) The changes in diameter of collagen gels in the absence (◆, control) or presence of Y-27632 at 1 (■), 10 (▲) or 100 (●) μM were measured. Data shown as mean±S.D. ($n=3$) were analysed by Student's t-tests. *$p<0.001$ versus control.

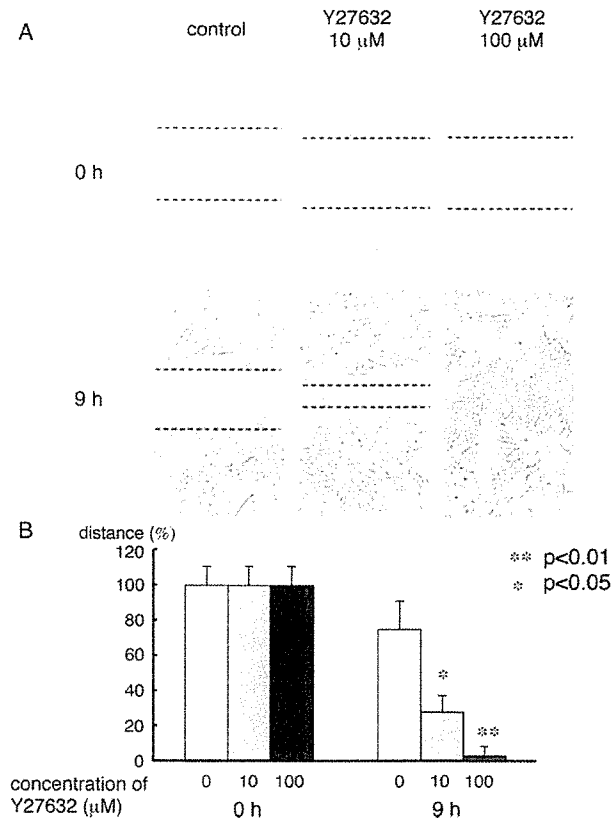

Fig. 6. Effect of Y-27632 on wound healing (motility) activities of human TM cells. (A) The cells grown to confluence were scraped with a yellow pipet tip to create a cell-free line. The medium was replaced with fresh medium without (control) or with 10 or 100 μM Y-27632. After 9 hr, migration of cells into the scraped area was photographed. The edges of migrated cells were indicated as dot lines. (B) The distances between the edges of migrated cells were measured, set at 100% before treatment, and shown as mean±S.D. ($n=3$). Data were analysed by Student's t-test.

phosphorylated LIM kinase 2 and phosphorylated cofilin (Fig. 7). However, The level of phosphorylated LIM kinase 1 and total cofilin remained unaffected. The observed changes in the phosphorylated forms of LIM kinase 2 and cofilin were reversible after a 2-hr recovery period.

4. Discussion

The present study demonstrates that a specific inhibitor of the ROCK/ROK family of protein kinases, Y-27632, induces profound changes in various behaviours of cultured human TM cells. Exposure to Y-27632 results in cell retraction and rounding of cell bodies with protrusions. Despite these changes, Y-27632 is found not to be toxic. It does not induce cell death nor inhibit proliferation in TM cells.

Our results reveal that TM cellular adhesiveness to the ECM is enhanced by Y-27632. This finding is somewhat unexpected, since in our previous study (Honjo et al., 2001) a decreased focal adhesion formation and loss of actin stress fibres in TM cells were noted after treatment of this inhibitor. The actin cytoskeleton is known to interact with

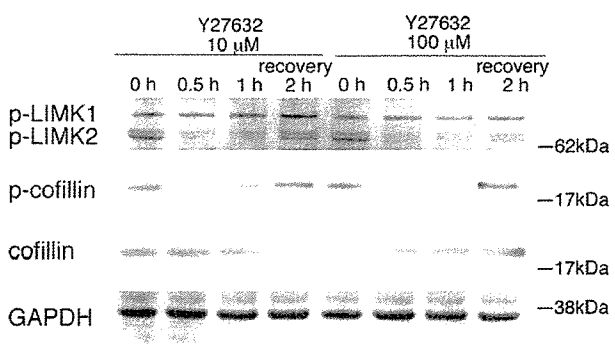

Fig. 7. Effects of Y-27632 on phosphorylation of LIM kinases and that of cofilin in human TM cells. Lysates were collected from cells untreated (control), or treated with 10 or 100 μM Y-27632 for 0.5 or 1 hr. Some dishes, after treatment of 10 or 100 μM Y-27632 for 1 hr, were incubated with fresh culture medium for an additional 2 hr (recovery 2 hr). Immunoblot analysis was performed for phosphorylated LIM kinase 1, phosphorylated LIM kinase 2, and phosphorylated and total cofilin. The levels of these proteins were normalized against that of GAPDH. Experiments were repeated 3 times, yielding similar results.

integrins to regulate cell shape and adhesiveness of cells to the matrix. In experiments using cultured THP-1 monocytes, inhibition of ROCK with Y-27632 did promote integrin adhesion that was accompanied by increases in membrane protrusions and phosphotyrosine signalling (Worthylake and Burridge, 2003). Similarly, in the present study, membrane protrusions were found in human TM cells after Y27632 treatment (data not shown). In addition, phosphotyrosine signalling and focal adhesion-associated molecules were concentrated at periphery of these protrusions by our immunocytochemical analysis (data not shown). The increased cell adhesiveness to ECM might be related to alterations in the cell shape and re-distribution of focal adhesions (and phosphotyrosine signalling) to the cell periphery.

Recent studies have indicated that cytoskeletal drugs including ROCK inhibitor decrease aqueous outflow resistance by destroying or stabilizing a complex of cytoplasmic fibres (Tian et al., 2000). Also, many cytoskeletal drugs have been reported to impair the adhesiveness of cell–cell or cell-matrix. For example, latrunculin-A was reported to be attenuated cell–cell attachments in human TM cells by immunocytochemical analysis (Cai et al., 2000). Protein kinase C inhibitor, which disrupt the actomyosin system, impair TM cell adhesion to ECM by quantitative adhesion assay (Zhou et al., 2000). In our study, protein expression level and distribution of cell–cell associated molecules such as β-catenin and pan-cadherin were almost unchanged after Y27632 treatment. Interestingly, adhesive activity to ECM was increased by the addition of Y27632. Decrease of the number of TM cells, that was observed in glaucomatous eyes, has been thought to be associated with decreased outflow facility and increased IOP (Rohen, 1983; Alvarado et al., 1984; Alvarado et al., 1986). The increased cellular adhesiveness to ECM by Y-27632 may prevent human TM cell decrease from TM tissues in glaucomatous eyes and can distinguish this inhibitor from other cytoskeletal drugs or inhibitors.

Contraction and relaxation of TM tissue are thought to control IOP (Thieme et al., 2000; Nakamura et al., 2002; Nakamura et al., 2003). In a previous study using bovine TM strips, Y27632 reduced TM tissue contraction (Thieme et al., 2000). In the present study, to investigate the direct effect of Y27632 on TM cellular contraction, we used three-dimensional cultures of human TM cells embedded in collagen type I gels. Gel contraction experiments reveal that addition of Y-27632 caused decreased contraction of collagen type I gel by TM cells. This phenomenon suggests reduced cell contractility and/or altered interaction between TM cells and collagen type I. However, as cell adhesion to collagen type I is found increased by addition of Y27632, the gel contraction change is thought to be due to just the TM cell relaxation by Y27632.

Administration of Y-27632, in addition, is shown to enhance motility of TM cells into the wound. This is in accordance with the notion that stabilization of actin stress fibres limits cell movement. Y-27632 also diminished the phosphorylation levels of LIM kinase 2 and cofilin. LIM kinase is the LIM domain-containing serine/threonine/tyrosine kinase composed of closely related LIM kinase 1 and LIM kinase 2 (Okano et al., 1995). They are known to be targets downstream of signalling by Rho GTPases. ROCK, specifically, has been shown to activate LIM kinase 2, but not LIM kinase 1 (Sumi et al., 2001). ROCK phosphorylates and activates LIM kinase 2, which phosphorylates and inactivates cofilin to suppress its actin-depolymerization and actin-severing activity, facilitating stress fibre formation (Bamburg, 1999). Consistent with this model, current experiments indicate that ROCK inhibitor Y-27632 reduces the levels of phosphorylated LIM kinase 2 and cofilin, not LIM kinase 1. The resulting dephosphorylated or active cofilin may in turn in TM cells promote actin depolymerization, formation of cell protrusions, and cell motility. These results suggest that the action of Y-27632 is, at least in part, mediated through the ROCK/LIM kinase 2/cofilin pathway. In previous reports, glucocorticoid, known to decrease aqueous outflow and cause secondary glaucoma, inhibits migration activities of TM cells (Clark et al., 1994). Furthermore, myocilin, known as a gene linked to both juvenile and adult-onset open angle glaucoma, also reduces migration activities of TM cells (Wentz-Hunter et al., 2004). In contrast, interestingly, our study revealed that Y-27632, an IOP lowering drug, accelerated migration activities of TM cells. Taken together, inhibition of migration activities might be associated with decreased aqueous outflow. However, further studies are required to reveal the association of migration activities and outflow facility.

In summary, the present study shows that Y-27632, a selective ROCK inhibitor, alters cellular behaviours of TM cells. It induces a reversible change in cell shape, increases cell adhesion, inhibits gel contraction, and accelerates cell migration. The IOP-lowering effect of Y-27632 observed in animal and perfusion organ culture studies (Honjo et al., 2001; Rao et al., 2001) is thus concluded to be related to the induced changes of TM cellular activities. Also, outflow facility was increased with gene transfer of dominant negative Rho A (Vittitow et al., 2002) or dominant negative binding domain of Rho-kinase (Rao et al., 2005) in anterior segments. The current data further specify that contractility in TM and/or Schlemm's canal cells may be a major factor in the physiology and regulation of the aqueous outflow, and that Rho/ROCK signal transduction is a key mediator of the cell contractility or relaxation. So far there have been accumulating data alluding to the usefulness of ROCK inhibitors as promising drugs in modulating the contractility of cells and lowering the IOP. The lack of toxicity of Y-27632, as demonstrated herein, offers an extra advantage in developing this inhibitor to be a therapeutic means for treatment of glaucoma.

Acknowledgements

This study was supported in part by a Grant-in-Aid for Scientific Research from the Ministry of Education, Science, Sports and Culture, Japan from the Ministry of Health and Welfare, Japan, and grants EY 05628 (BYJTY) and EY 01792 (core) from the National Eye Institute, Bethesda, MD, USA. The authors thank Professor Shuh Narumiya, Department of Pharmacology Kyoto University Faculty of Medicine for his kind advice.

References

Alvarado, J., Murphy, C., Polansky, J., Juster, R., 1981. Age-related changes in trabecular meshwork cellularity. Invest. Ophthalmol. Vis. Sci. 21, 714–727.

Alvarado, J., Murphy, C., Juster, R., 1984. Trabecular meshwork cellularity in primary open-angle glaucoma and nonglaucomatous normals. Ophthalmology 91, 564–579.

Alvarado, J.A., Yun, A.J., Murphy, C.G., 1986. Juxtacanalicular tissue in primary open angle glaucoma and in nonglaucomatous normals. Arch. Ophthalmol. 104, 1517–1528.

Bamburg, J.R., 1999. Proteins of the ADF/cofilin family: essential regulators of actin dynamics. Annu. Rev. Cell Dev. Biol. 15, 185–230.

Bill, A., Phillips, C.I., 1971. Uveoscleral drainage of aqueous humor in human eyes. Exp. Eye Res. 12, 275–281.

Cai, S., Liu, X., Glasser, A., Volberg, T., Filla, M., Geiger, B., Polansky, J.R., Kaufman, P.L., 2000. Effect of latrunculin-A on morphology and actin-associated adhesions of cultured human trabecular meshwork cells. Mol. Vis. 6, 32–43.

Choi, J., Miller, A.M., Nolan, M.J., Yue, B.Y.J.T., Thoz, S.T., Clark, A.F., Agarwal, N., Knepper, P.A., 2005. Soluble CD44 is cytotoxic to trabecular meshwork and retinal ganglion cells in vitro. Invest. Ophthalmol. Vis. Sci. 46, 214–222.

Clark, A.F., Wilson, K., McCartney, M.D., Miggans, S.T., Kunkle, M., Howe, W., 1994. Glucocorticoid-induced formation of cross-linked actin networks in cltured human trabecular meshwork cells. Invest. Ophthalmol. Vis. Sci. 35, 281–294.

Epstein, D.L., Freddo, T.F., Bassett-Chu, S., Chung, M., Karageuzian, L., 1987. Influence of ethacrynic acid on outflow facility in the monkey and calf eye. Invest. Ophthalmol. Vis. Sci. 28, 2067–2075.

Epstein, D.L., Rowlette, L.L., Roberts, B.C., 1999. Acto-myosin drug effects and aqueous outflow function. Invest. Ophthalmol. Vis. Sci. 40, 74–81.

Honjo, M., Tanihara, H., Inatani, M., Kido, N., Sawamura, T., Yue, B.Y.J.T., Narumiya, S., Honda, Y., 2001. Effects of Rho-associated protein kinase inhibitor Y-27632 on intraocular pressure and outflow facility. Invest. Ophthalmol. Vis. Sci. 42, 137–144.

Ishizaki, T., Maekawa, M., Fujisawa, K., Okawa, K., Iwamatsu, A., Fujita, A., Watanabe, N., Saito, Y., Kakizuka, A., Morii, N., Narumiya, S., 1996. The small GTP-binding protein Rho binds to and activates a 160 kDa Ser/Thr protein kinase homologous to myotonic dystrophy kinase. EMBO J. 15, 1885–1893.

Jain, P.T., Pento, J.T., Graves, D.C., 1992. Cell-growth quantitation methods for the evaluation of antiestrogens in human breast cancer cells in culture. J. Pharmacol. Toxicol. Methods 27, 203–207.

Jocson, V.L., Sears, M.L., 1971. Experimental aqueous perfusion in enucleated human eyes. Results after obstruction of Schlemm's canal. Arch. Ophthalmol. 86, 65–71.

Kaibuchi, K., Kuroda, S., Amano, M., 1999. Regulation of the cytoskeleton and cell adhesion by the Rho family GTPases in mammalian cells. Annu. Rev. Biochem. 68, 459–486.

Kaufman, P.L., Barany, E.H., 1977. Cytochalasin B reversibly increases outflow facility in the eye of the cynomolgus monkey. Invest. Ophthalmol. Vis. Sci. 16, 47–53.

Kaufman, P.L., Erickson, K.A., 1982. Cytochalasin B and D dose-outflow facility response relationships in the cynomolgus monkey. Invest. Ophthalmol. Vis. Sci. 23, 646–650.

Khurana, R.N., Deng, P.F., Epstein, D.L., Rao, P.V., 2003. The role of protein kinase C in modulation of aqueous humor outflow facility. Exp. Eye Res. 76, 39–47.

Knepper, P.A., Goossens, W., Hvizd, M., Palmberg, P.F., 1996. Glycosaminoglycans of the human trabecular meshwork in primary open-angle glaucoma. Invest. Ophthalmol. Vis. Sci. 37, 1360–1367.

Leung, T., Manser, E., Tan, L., Lim, L., 1995. A novel serine/threonine kinase binding the Ras-related RhoA GTPase which translocates the kinase to peripheral membranes. J. Biol. Chem. 270, 29051–29054.

Lutjen-Drecoll, E., Gabelt, B.T., Tian, B., Kaufman, P.L., 2001. Outflow of aqueous humor. J. Glaucoma. 10, S42–S44.

Matsui, T., Amano, M., Yamamoto, T., Chihara, K., Nakafuku, M., Ito, M., Nakano, T., Okawa, K., Iwamatsu, A., Kaibuchi, K., 1996. Rho-associated kinase, a novel serine/threonine kinase, as a putative target for small GTP binding protein Rho. EMBO J. 15, 2208–2216.

McMenamin, P.G., Lee, W.R., Aitken, D.A., 1986. Age-related changes in the human outflow apparatus. Ophthalmology 93, 194–209.

Miyazaki, M., Segawa, K., Urakawa, Y., 1987. Age-related changes in the trabecular meshwork of the normal human eye. Jpn. J. Ophthalmol. 31, 558–569.

Nakagawa, O., Fujisawa, K., Ishizaki, T., Saito, Y., Nakao, K., Narumiya, S., 1996. ROCK-I and ROCK-II, two isoforms of Rho-associated coiled-coil forming protein serine/threonine kinase in mice. FEBS Lett. 39, 189–193.

Nakamura, Y., Hirano, S., Suzuki, K., Seki, K., Sagara, T., Nishida, T., 2002. Signaling mechanism of TGF-β1-induced collagen contraction mediated by bovine trabecular meshwork cells. Invest. Ophthalmol. Vis. Sci. 43, 3465–3472.

Nakamura, Y., Sagara, T., Seki, K., Hirano, S., Nishida, T., 2003. Permissive effect of fibronectin on collagen gel contraction mediated by bovine trabecular meshwork cells. Invest. Ophthalmol. Vis. Sci. 44, 4331–4336.

Nobes, C.D., Hall, A., 1995. Rho, Rac and cdc42 GTPases: regulators of actin structures, cell adhesion and motility. Biochem. Soc. Trans. 23, 456–459.

Okano, I., Hiraoka, J., Otera, H., Nunoue, K., Ohashi, K., Iwashita, S., Hirai, M., Mizuno, K., 1995. Identification and characterization of a novel family of serine/threonine kinases containing two N-terminal LIM motifs. J. Biol. Chem. 270, 31321–31330.

Rao, P.V., Deng, P.F., Kumar, J., 2001. Epstein DL. Modulation of aqueous humor outflow facility by the Rho kinase-specific inhibitor Y-27632. Invest. Ophthalmol. Vis. Sci. 42, 1029–1037.

Rao, P.V., Deng, P., Maddala, R., Epstein, D.L., Li, C.Y., Shimokawa, H., 2005. Expression of dominant negative Rho-binding domain of Rho-kinase in organ cultured human eye anterior segments increases aqueous humor outflow. Mol Vis. 11, 288–297.

Riento, K., Ridley, A.J., 2003. ROCKs: multifunctional kinases in cell behavior. Nat. Rev. Mol. Cell Biol. 4, 446–456.

Rohen, J.W., 1983. Why is intraocular pressure elevated in chronic simple glaucoma? Anatomical considerations. Ophthalmology 90, 758–765.

Sawaguchi, S., Yue, B.Y.J.T., Chang, I.L., Wong, F., Higginbotham, E.J., 1992. Ascorbic acid modulates collagen type I gene expression by cells from an eye tissue-trabecular meshwork. Cell Mol. Biol. 38, 587–604.

Sumi, T., Matsumoto, K., Nakamura, T., 2001. Specific activation of LIM kinase 2 via phosphorylation of threonine 505 by ROCK, a Rho-dependent protein kinase. J. Biol. Chem. 276, 670–676.

Takai, Y., Sasaki, T., Tanaka, K., Nakanishi, H., 1995. Rho as a regulator of the cytoskeleton. Trends Biochem. Sci. 20, 227–231.

Thieme, H., Nuskovski, M., Nass, J.U., Pleyer, U., Strauss, O., Wiederholt, M., 2000. Mediation of calcium-Independent contraction in trabecular meshwork through protein kinase C and Rho-A. Invest. Ophthalmol. Vis. Sci. 41, 4240–4246.

Tian, B., Kaufman, P.L., Volberg, T., Gabelt, B.T., Geiger, B., 1998. H-7 disrupts the actin cytoskeleton and increases outflow facility. Arch. Ophthalmol. 116, 633–643.

Tian, B., Geiger, B., Epstein, D.L., Kaufman, P.L., 2000. Cytoskeletal involvement in the regulation of aqueous humor outflow. Invest. Ophthalmol. Vis. Sci. 41, 619–623.

Uehata, M., Ishizaki, T., Satoh, H., Ono, T., Kawahara, T., Morishita, T., Tamalawa, H., Yamagami, K., Inui, J., Maekawa, M., Narumiya, S., 1997. Calcium sensitization of smooth muscle mediated by a Rho-associated protein kinase in hypertension. Nature 389, 990–994.

Vittitow, J.L., Garg, R., Rowlette, L.L., Epstein, D.L., O'Brien, E.T., Borras, T., 2002. Gene transfer of dominant-negative RhoA increases outflow facility in perfused human anterior segment cultures. Mol Vis. 8, 32–44.

Wentz-Hunter, K., Kubota, R., Shen, X., Yue, B.Y.J.T., 2004. Extracellular myocilin affects activity of human trabecular meshwork cells. J. Cell Physiol. 200, 45–52.

Worthylake, R.A., Burridge, K., 2003. RhoA and ROCK promote migration by limiting membrane protrusions. J. Biol. Chem. 278, 13578–13584.

Yue, B.Y.J.T., Higginbotham, E.J., Chang, I.L., 1990. Ascorbic acid modulates the production of fibronectin and laminin by cells from an eye tissue-trabecular meshwork. Exp. Cell Res. 187, 65–68.

Zhou, L., Zhang, S.R., Yue, B.Y., 1996. Adhesion of human trabecular meshwork cells to extracellular matrix proteins. Roles and distribution of integrin receptors. Invest. Ophthalmol. Vis. Sci. 37, 104–113.

Zhou, L., Cheng, E.L., Rege, P., Yue, B.Y.J.T., 2000. Signal transduction mediated by adhesion of human trabecular meshwork cells to extracellular matrix. Exp. Eye Res. 70, 457–465.

Graefe's Arch Clin Exp Ophthalmol
(2006) 244: 1056–1059

SHORT COMMUNICATION

DOI 10.1007/s00417-005-0238-6

Yuki Mawatari
Akira Hirata
Mikiko Fukushima
Hidenobu Tanihara

Choroidal dye filling velocity in patients with Vogt–Koyanagi–Harada disease

Received: 14 January 2005
Accepted: 11 April 2005
Published online: 13 January 2006

Y. Mawatari · A. Hirata (✉) ·
M. Fukushima · H. Tanihara
Department of Ophthalmology and
Visual Science, Kumamoto University
Graduate School of Medical Sciences,
1–1–1 Honjo,
Kumamoto, 860-8556, Japan
e-mail: ahirata@apost.plala.or.jp
Tel.: +81-96-373-5247
Fax: +81-96-373-5249

Abstract *Purpose:* To evaluate quantitative choroidal dye filling velocity in patients with Vogt-Koyanagi-Harada disease (VKH) before and after corticosteroid treatment using indocyanine green (ICG) angiography. *Methods:* ICG angiography was performed in seven VKH patients before and after systemic corticosteroid treatment. Choroidal dye curves were obtained by image analysis software and analyzed using an exponential model. The model's time constant (τ) was used to evaluate choroidal dye filling velocity. *Results:* Compared with controls, acute phase choroidal τ values in VKH patients were significantly longer, suggesting choroidal circulation disturbance. During the recovery phase, choroidal τ values were significantly shortened, suggesting choroidal circulatory disturbance improvement. *Conclusion:* Choroidal dye filling velocity may be useful for VKH diagnosis and verification of corticosteroid treatment effectiveness.

Introduction

Vogt-Koyanagi-Harada disease (VKH) is characterized by bilateral panuveitis and systemic autoimmune disease with skin manifestations such as vitiligo and alopecia, hearing disturbances such as dysacousis and tinnitus, and meningeal signs [6]. Several studies have described characteristic ophthalmologic and angiographic findings of VKH [1, 5, 7–9, 12]. Fluorescein angiography in the acute phase of VKH has documented an area of hypofluorescence, with an early phase multiple pinpoint area of leakage and a late phase large confluent area of leakage. With indocyanine green (ICG) angiography, decreased background fluorescence and delayed filling is observed in the early phases of acute phase VKH, suggesting choroidal circulation disturbance. Corticosteroid treatment reverses these changes.

With the introduction of scanning laser ophthalmoscopes and image analyses, dye filling curves are more readily available. Using these curves, retinal and choroidal hemodynamics data have been obtained [2, 3, 11].

Choroidal circulation disturbances occur in the acute phase of VKH [1, 5, 7, 8, 12]. However, quantitative assessment of choroidal circulation has not been clarified. Therefore, we measured choroidal dye filling velocity before and after corticosteroid treatment, and investigated clinical significance.

Materials and methods

Patients

Seven patients (three males, four females) referred to and diagnosed with VKH at Kumamoto University Hospital between March 2002 and April 2003 were studied. Diagnosis was based on clinical history and ophthalmologic and related examinations, including fluorescein and ICG angiography. Patients with other systemic and ocular diseases were excluded. The mean age was 40.7±12.7 (SD) years (range 21–54 years). The mean follow-up period was 14.4±5.0 (SD) months (range, 7–20 months). Usual VKH treatments were administered with all subjects receiving intravenous betamethasone (20 mg/day to 10 mg/day over 10 days) followed by oral prednisolone with cautious tapering (60 mg/day to 5 mg/day over 3 months). Prior to treatments, informed

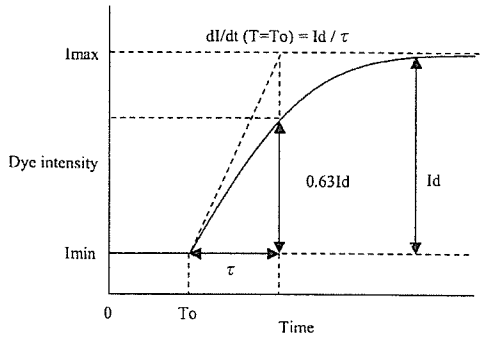

$$I(t) = Imin \quad ; 0 < T < To$$
$$= Id\{1 - EXP^{-(T-To/\tau)}\} \quad ; T \geq To$$

Imin = background intensity before appearance of the dye; To = time at the start point of the filling curves; Id = Imax – Imin, and reflects the blood volume; Imax = maximal intensity of the curve; EXP = exponent with e as the base ≅ 2.72; τ (tau) = the time constant of this model.

$$dI/dt = Id/\tau \, EXP^{-(T-To/\tau)}$$
dye filling velocity $= dI/dt \; (T = To)$
$$= Id/\tau$$

τ corresponds to the time of 0.63 Id of the dye curve ($1-e^{-1} \cong 0.63$).

Fig. 1 The graphical representation of the model curve used to analyze the individual dye filling curves (modified from previous report by Duijm et al. [2, 3]). The time course is described by four parameters: background intensity before appearance of the dye (*Imin*), maximal intensity of the curve (*Imax*), time at the onset of the filling curves (*To*), time constant of the model (τ)

consent was obtained from all patients in this study. Fluorescein and ICG angiography using a scanning laser ophthalmoscope (Rodenstock Instrument, Inc., Munich, Germany) were performed before initiation of, and 2 weeks and 3 months after the corticosteroid treatments. Additional angiography was performed 1 month after corticosteroid treatment in one patient suffering recurrence. As previous studies have demonstrated that the choroidal blood flow and ocular perfusion pressure relationship is linear in a certain range, each patient's blood pressure and intraocular pressure (IOP) were measured before angiograms [10]. Average ocular perfusion pressure was defined as:

$$\text{perfusion pressure} = \text{Pdiastolic} + 1/3(\text{Psystolic} - \text{Pdiastolic}) - \text{IOP}$$

Early phase angiograms were performed on one selected eye before and after corticosteroid treatment. For fluorescein angiography, 5 ml of a 10% sodium fluorescein solution was rapidly injected into the cubital vein. After fluorescein staining, 50 mg of dye (Diagnogreen; Daiichi Pharmaceutical, Inc., Tokyo, Japan) dissolved in 5 ml distilled water solution was injected into the cubital vein and ICG angiography performed. Data from angiography were analyzed using the image analysis software (DIPP-Motion2D, DITECT, Japan). The averaged intensity of targeted areas was obtained every 1/30 s and a choroidal dye curve was constructed using the software.

Controls consisted of 15 randomly selected healthy control subjects matched for age and gender. Each underwent ICG angiography after injection of 50 mg dye.

Measurement of choroidal dye filling velocity

Fluorescein angiography use in analysis of choroidal circulation has previously been presented [2, 3, 11]. We applied the same method and used ICG angiography to construct choroidal dye intensity curves. The curves were analyzed according to an exponential model shown in Fig. 1. If dye filling velocity decreases, the time constant (τ) increases. In a preliminary study, we found the choroidal τ value remained constant even when the type of dye injection changed (unpublished data from YM).

In this study, choroidal dye filling velocity was measured on macular areas that were three disk diameters in diameter and excluded large retinal vessels. The τ of each area measured was averaged.

Table 1 Clinical characteristics of VKH patients

Patient no.	Age (years)	Gender	Before treatment			After treatment					
						2 weeks			3 months		
			τ	VA	SRD	τ	VA	SRD	τ	VA	SRD
1	43	F	4.6	20/200	+	3.1	20/25	-	2.6	20/15	-
2	21	F	4.2	20/200	+	3.3	20/30	-	3.5	20/15	-
3	53	M	6	20/70	+	3.6	20/40	+	4.2	20/20	-
4	49	F	5.3	20/25	+	3.5	20/15	-	3.8	20/15	-
5	37	M	5.7	20/15	-	2.6	20/15	-	3.2	20/15	-
6	54	M	5.4	20/500	+	6.5	20/100	-	3.9	20/20	-
7	28	F	5.5	20/50	+	3.1	20/20	+	3.8	20/20	-

VA visual acuity; *SRD* serous retinal detachment

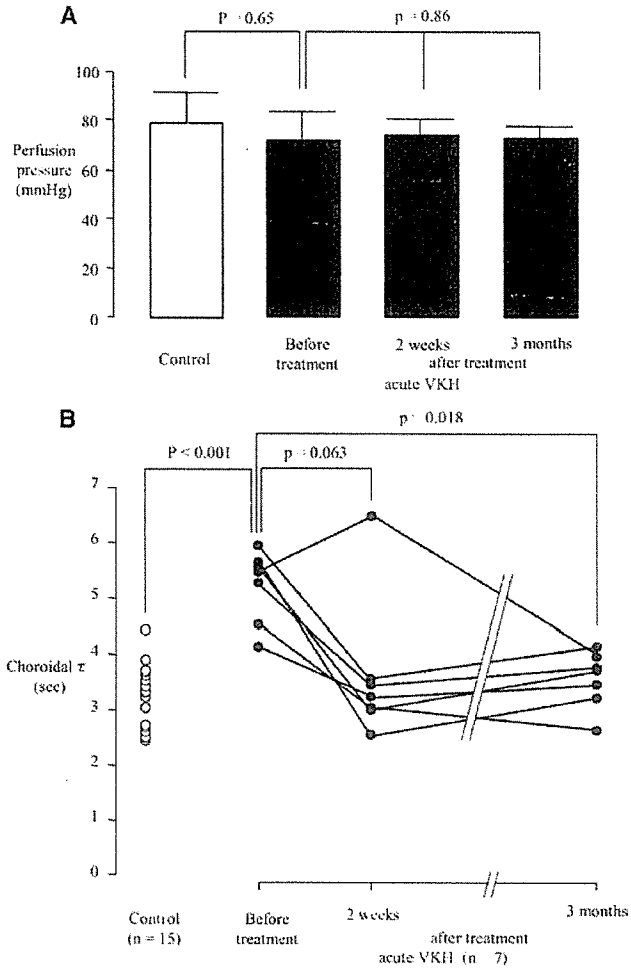

Fig. 2 Perfusion pressure and choroidal τ between control and acute VKH. **a** Compared with control, there is no difference in perfusion pressure in acute VKH. Perfusion pressure in patients with VKH was constant throughout corticosteroid therapy. **b** Compared with control, choroidal τ values in patients with acute VKH were significantly longer. Only in one patient (no. 6) was the choroidal τ value still longer at 2 weeks after corticosteroid treatment. Choroidal τ was significantly shortened in all patients at 3 months after corticosteroid treatment

Statistical analysis

Data were presented as the mean (minimal–maximal value). To compare the differences between controls and the seven acute phase VKH patients for the ocular perfusion pressure and the τ, we used an unpaired *t*-test and a Mann–Whitney *U*-test, respectively. Differences in ocular perfusion pressure before and 2 weeks and 3 months after corticosteroid treatment in the seven VKH patients were compared using repeated ANOVA and Wilcoxon signed rank sum tests. The differences in τ before and 2 weeks and 3 months after corticosteroid treatment in the seven VKH patients were compared using the Friedman test. *P*-values less than 0.05 were considered statistically significant.

Table 2 Clinical characteristics of control and VKH in acute phase

	Age (years)	Gender male : female	Perfusion pressure	τ
Control (*n*=15)	43.7±12.4 (28-59)	9:6	76.7±10.1 (55.0-92.3)	3.2±0.6 (2.4-4.4)
VKH in acute phase (*n*=7)	40.7±12.7 (21-54)	4:3	72.3±5.4 (68.0-80.0)	5.2±0.6 (4.2-6.0)

Results

In controls (*n*=15) matched for age and gender, average choroidal τ was 3.2 (2.4–4.4) s (Table 2). In the seven VKH acute phase patients, average choroidal τ was 5.2 (4.2–6.0) s, which was significantly longer compared to controls (Table 1, Fig. 2). There were no differences in ocular perfusion pressure between controls and the seven acute phase VKH patients (*P*=0.65, Table 2, Fig. 2a).

Except for subject 6, choroidal τ was shortened in all patients 2 weeks after corticosteroid treatment (Table 1, Fig. 2b). Ophthalmologic findings for this patient indicated vascular leakage during fluorescein angiography. At 2 weeks after corticosteroid treatment, an improved choroidal background was seen with ICG angiography. However, during the tapering of the corticosteroid, the patient suffered recurrence of serous retinal detachment. With increased corticosteroid administration, choroidal dye filling velocity shortened and the serous retinal detachment disappeared. In patients 3 and 7, choroidal τ values shortened without disappearance of serous retinal detachment 2 weeks after treatment (Table 1). However, the serous retinal detachments disappeared during the following week.

In the VKH recovery phase (3 months after corticosteroid treatment), choroidal τ values were significantly shortened without any noted changes in ocular perfusion pressure (*P*=0.018, Table 1, Fig. 2).

Discussion

In this study, we quantitatively measured choroidal circulation using ICG angiography and image analysis software. Previous studies have used fluorescein angiography to analyze choroidal circulation [2, 3, 11]. We applied this method using ICG angiography, as it reflects choroidal circulation better than fluorescein. Furthermore, we used a new type of image analysis software (DIPP-Motion 2D), which allows the dye intensity curve to easily be obtained (approximately 5–10 min per angiogram to obtain the data/curve).